Taibah University

**Journal of Taibah University Medical Sciences**

Original Article

# Molecular properties and In silico bioactivity evaluation of (4-fluorophenyl)[5])-3-phen-(4-nitrophenyl yl-4,5-dihydro-1$H$-pyrazol-1-yl]methanone derivatives: DFT and molecular docking approaches

Ibrahim A. Omotayo, PhD [a], Semire Banjo, PhD [a,*], Oladuji T. Emmanuel, PhD [a], Latona D. Felix, PhD [b], Oyebamiji A. Kolawole, PhD [c], Owonikoko A. Dele, PhD [d], Abdulsalami I. Olasegun, PhD [e], Adeoye M. Dasola, PhD [f] and Odunola O. Ayobami, PhD [a,g]

[a] *Computational Chemistry Laboratory, Department of Pure and Applied Chemistry, Ladoke Akintola University of Technology, Ogbomoso, Nigeria*
[b] *Department of Pure and Applied Chemistry, Osun State University, Osogbo, Nigeria*
[c] *Department of Chemistry and Industrial Chemistry, Bowen University, Iwo, Nigeria*
[d] *Department of Chemistry, Emmanuel Alayande College of Education, Nigeria*
[e] *Department of Chemistry, Nigerian Army University, Biu, Nigeria*
[f] *Department of Chemical Sciences, Fountain University, Osogbo, Nigeria*
[g] *Department of Chemistry, Faculty of Natural and Applied Sciences, Hallmark University, Ijebu-Itele, Nigeria*

**المخلص**

تمت دراسة سلسلة من مشتقات الميثانون (4-فلوروفينيل) [5]- (4-نيتروفينيل) -3-فينيل-5،4-ثنائي هيدرو-1اتش-بيرازول-1-يل] باستخدام الطرق الحسابية. تم إجراء تحسين التوازن لهذه المركبات عند مستوى "ب3ليب/6-31ج**" من الناحية النظرية، وتم التنبؤ بالمعلمات الهندسية، والاهتزاز الترددي، وخصائص الأشعة المرئية وفوق البنفسجية على أساس حسابات نظرية الكثافة الوظيفية. كشفت فجوة الطاقة، والتبرع بالإلكترون / قبول الطاقة واستجابة كثافة الإلكترون تجاه الإلكتروفيل / النوكليوفيل المحسوبة لـ إم1 و إم2، عن أهمية وضع البديل على السلوك الكيميائي للمركب. أيضا، أظهر التبرع بالإلكترون / قبول الطاقة و فجوة الطاقة أن إم6 أكثر إلكتروفيلا بسبب وجود مجموعتين من "إن أو 2"، مما يعزز خصائص "إن إل أو" الخاصة به. تراوحت قابلية الاستقطاب المفرط للمركبات 5.21-7.26 × 10⁻³⁰ وحدة كهرباء وكانت أكبر من مادة اليوريا القياسية "إن إل أو"؛ وبالتالي جعل إم1-إم6 مرشحين محتملين لتطبيقات "إن إل أو". كشفت عمليات محاكاة الإرساء أن التقاربات الملزمة للمركبات الستة

تراوحت من -8.8 إلى -9.3 كيلو كالوري / مول لـ "أ ب أو"-نازعة هيدروجين الكبد (عنوان بي دي بي: 5 أ دي إتش) و -8.5 إلى -9.7 كيلو كالوري / مول لـ هيدرولاز البروتين المضاد للالتهابات (عنوان بي دي بي: 1 آر أو 6)؛ وبالتالي يمكن أن تمتلك خصائص جيدة مضادة للأكسدة ومضادة للالتهابات.

**الكلمات المفتاحية:** ميثانون (4-فلوروفينيل) [5]- (4-نيتروفينيل) -3-فينيل-5،4-ثنائي هيدرو-1اتش-بيرازول-1-يل]؛ نظرية الكثافة الوظيفية؛ إرساء جزيئي

**Abstract**

**Objectives:** Molecular structures, spectroscopic properties, charge distributions, frontier orbital energies, nonlinear optical (NLO) properties and molecular docking simulations were analyzed to examine the biousefulness of a series of (4-fluorophenyl)[5-(4-nitrophenyl)-3-phenyl-4,5-dihydro-1H-pyrazol-1-yl] methanone derivatives.

**Methods:** The compounds were studied through computational methods. Equilibrium optimization of the compounds was performed at the B3LYP/6-31G(d,p) level of theory, and geometric parameters, frequency vibration, UV−vis spectroscopy and reactivity properties were predicted on the basis of density functional theory (DFT) calculations.

* Corresponding address: Computational Chemistry Laboratory, Department of Pure and Applied Chemistry, Ladoke Akintola University of Technology, P.M.B. 4000, Ogbomoso, Oyo-State, Nigeria

E-mail: bsemire@lauctech.edu.ng (S. Banjo)

ELSEVIER **Production and hosting by Elsevier**

**Results:** The energy gap (ΔEg), electron donating/accepting power (**ω−/ω+**) and electron density response toward electrophiles/nucleophiles calculated for **M1** and **M2** revealed the importance of substituent positioning on compound chemical behavior. In addition, **ω−/ω+** and ΔEn/ΔEe indicated that **M6** is more electrophilic because of the presence of two NO$_2$ groups, which enhanced its NLO properties. The hyperpolarizability (β$_0$) of the compounds ranged from $5.21 \times 10^{-30}$ to $7.26 \times 10^{-30}$ esu and was greater than that of urea; thus, **M1−M6** were considered possible candidates for NLO applications. Docking simulation was also performed on the studied compounds and targets (PDB ID: 5ADH and 1RO6), and the calculated binding affinity and non-bonding interactions are reported.

**Conclusion:** The calculated ω$^−$ and ω$^+$ indicated the electrophilic nature of the compounds; **M6**, a compound with two NO$_2$ groups, showed enhanced effects. Molecular electrostatic potential (MEP) analysis indicated that amide and nitro groups on the compounds were centers of electrophilic attacks. The magnitude of the molecular hyperpolarizability suggested that the entire compound had good NLO properties and therefore could be explored as a candidate NLO material. The docking results indicated that these compounds have excellent antioxidant and anti-inflammatory properties.

**Keywords:** DFT; Molecular docking; [5-(4-nitrophenyl)-3-phenyl-4,5-dihydro-1*H*-pyrazol-1-yl]methanone

## Introduction

Pyrazole derivatives are heterocyclic compounds recognized to possess a wide range of biological and pharmacological activities.[1,2] The unique properties of pyrazoles have been attributed to the electrophilic substitution reactions that occur specially at position 4, and nucleophilic attacks that occur at positions 3 and 5, thus leading to diverse pyrazole structures with broad potential applications in areas such as medicine, agriculture and technology.[3–5] In addition, compounds containing a pyrazole nucleus have been reported to be anti-inflammatory, antiviral, anticancer, antiparasitic, antibacterial, antirheumatoid, antidepressant, analgesic, antinociceptive, antihypertensive, antipyretic and antifungal agents.[6–12] Beyond these biological activities, this class of compounds displays substantial nonlinear optical (NLO) properties,[13–17] electroluminescent properties due to photo-induced-electron transfer,[18] and light amplification properties due to stimulated emission or lasing/random lasing action.[14,15]

Several pyrazole derivatives, such as 3-(1,1-dicyanoethenyl)-1-phenyl-4,5-dihydro-1*H*-pyrazole, have been investigated for their NLO properties. The size of the nano-crystals of the compound has been suggested to play a major role in the excitation or emission efficiency.[19,20] Thus,

these compounds can be used for ultrafast optics.[21] The optical nonlinearity of a series of *N*-substituted-5-phenyl-1*H*-pyrazole-4-ethyl carboxylates of compounds in chloroform solution has been assessed, and these compounds have been found to be good candidates for NLO applications.[22] In addition, a series of (*Z*)-2-(4-nitrophenyl)-3-(1-phenyl-4,5-dihydro-1*H*-pyrazol-3-yl)acrylonitrile and (*E*)-3-(4-nitrostyryl)-1-phenyl-4,5-dihydro-1*H*-pyrazole compounds have been found to have several electron accepting groups attached and to show high NLO responses dependent on functionalization of the pyrazoline derivatives.[23] The compounds 1-*N*-phenyl-3(3,4-dichlorophenyl)-5-phenyl-2-pyrazoline,[24] diethyl-1*H*-pyrazole-3,5-dicarboxylate and 4-(4-bromophenyl)-1-tert-butyl-3-methyl-1*H*-pyrazol-5-amine[25] have been studied with experimental and density functional theory (DFT) methods and found to have promising NLO properties.

More recently, DFT has been used in conformational and NBO analysis of (4-chloro-3,5-dimethyl-1*H*-pyrazol-1-yl)(p-tolyl)methanone, and the results have shown excellent agreement with experimental data.[26] Likewise, 2-bromo-*N*-(2,3-dihydro-1,5-dimethyl-3-oxo-2-phenyl-1*H*-pyrazol-4-yl)benzamide and 2-chloro-*N*-(2,3-dihydro-1,5-dimethyl-3-oxo-2-phenyl-1*H*-pyrazol-4-yl)benzamide have been studied with both experimental and DFT methods; the theoretical results have revealed that both compounds display energetic hydrogen bonding interactions and are stabilized by electrostatic energy contribution, in line with experimental observations.[27] Santhi and Bharathi have reported the synthesis and molecular structural elucidation of a series of 4-(3-(2-amino-3,5-dibromophenyl)-1-(benzoyl)-4,5-dihydro-1*H*-pyrazol-5-yl)benzonitriles through spectroscopic and DFT methods. The DFT method has been used to analyze the studied molecules' molecular electrostatic potential, natural bonding orbitals, Mulliken charges, frontier molecular orbital energies and NLO properties. The results have indicated inter- and intra-molecular delocalization and acceptor−donor interactions based on second-order perturbation interactions; moreover, polarizability and hyperpolarizability calculations have indicated that the compounds possess good NLO properties.[28]

In this work, DFT calculations were performed on 4-(3-(2-amino-3,5-dibromophenyl)-1-(benzoyl)-4,5-dihydro-1*H*-pyrazol-5-yl)benzonitriles reported by Santhi and Bharathi.[28] Structural modifications were used to design six new compounds, as shown in Table 1. The molecular structures, spectroscopic properties, charge distributions, frontier orbital energies, NLO properties and molecular docking simulations were analyzed to examine the bio-usefulness of the studied compounds.

## Theoretical details

Before DFT calculations, an equilibrium conformer search was performed on all compounds with a semi-empirical AM1 method to identify the lowest conformer for each compound, which was used for further DFT calculations.[29] All calculations were performed on these compounds with Becke's three parameter hybrid functional DFT, with Lee, Yang and Parr correlation,[30] and optimized at B3LYP/6-31G(d,p) level of theory in gas.

Frequency calculation was also performed by using the same basis set to confirm that the optimized molecules were minima, as characterized by positive harmonic frequencies[31,32] in Spartan 14.[33] The DFT hybrid B3LYP functional has been reported to overestimate the fundamental modes; however, this overestimation can be addressed by calculating harmonic frequencies with a scaling factor of 0.9619 to yield frequencies consistent with experimental data.[34] The molecular descriptors calculated from conceptual DFT were the ionization potential (I = −HOMO), electron affinity (A = −LUMO), chemical hardness (η), chemical potential (μ), global electrophilicity (ω), electron donating power (ω−), electron accepting power (ω+), nucleofugality (ΔE_n) and electrofugality (ΔE_e) (equations (1)−(7)).[35−39]

$$\mu = \frac{-E_{LUMO} + E_{HOMO}}{2} \approx \frac{I + A}{2} \qquad 1$$

$$\mu = -\frac{E_{HOMO} + E_{LUMO}}{2} \approx \frac{I + A}{2} \qquad 2$$

$$\omega = \frac{\mu^2}{2\eta} = \frac{(I+A)^2}{4(I-A)} \qquad 3$$

$$\omega^- = \frac{(3I+A)^2}{16(I-A)} \qquad 4$$

$$\omega^+ = \frac{(I+3A)^2}{16(I-A)} \qquad 5$$

$$\Delta E_n = -A + \omega = \frac{(\mu+\eta)^2}{2\eta} \qquad 6$$

$$\Delta E_e = I + \omega = \frac{(\mu-\eta)^2}{2\eta} \qquad 7$$

### Results and discussion

*Geometry parameters*

The geometry parameters extracted from the equilibrium structures optimized at the B3LYP/6-31G(d,p) level for the six compounds **M1−M6** are displayed in Tables 2 and 3. The results were compared with the geometries of 4-(3-(2-amino-3,5-dibromophenyl)-1-(4-nitrobenzoyl)-4,5-dihydro-1*H*-pyrazol-5-yl)benzonitrile predicted at the same level of theory.[28] The calculated C3−N7 bonds were 1.299, 1.298, 1.300, 1.299, 1.299 and 1.298 Å for **M1−M6**, respectively, in agreement with the 1.299 Å calculated for **Ma**. This type of bond has been experimentally observed to be 1.275 Å and calculated to be 1.287 Å for bis-spiropipridinon/pyrazole derivatives.[40] The C1−N8 bond in the pyrazole ring displayed a typical single bond character with a bond length of 1.482 Å
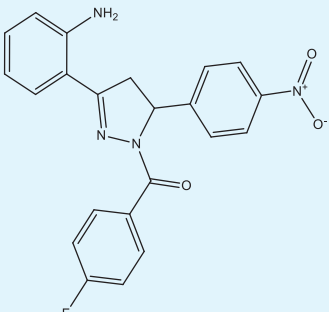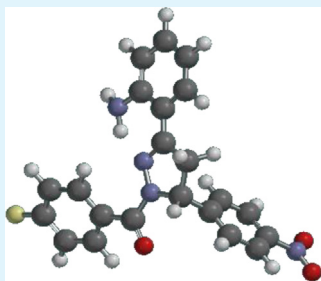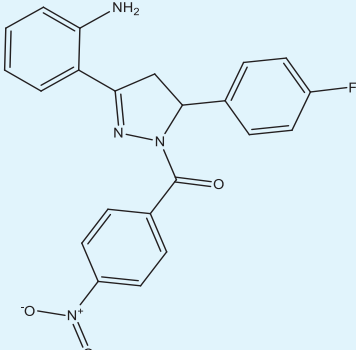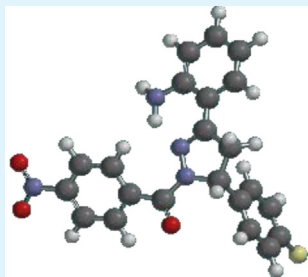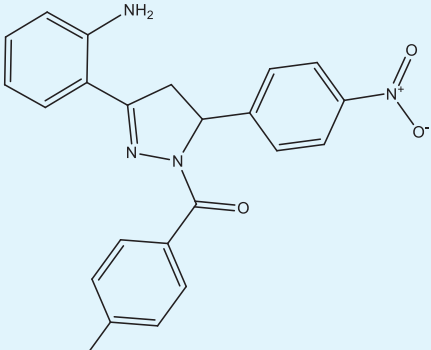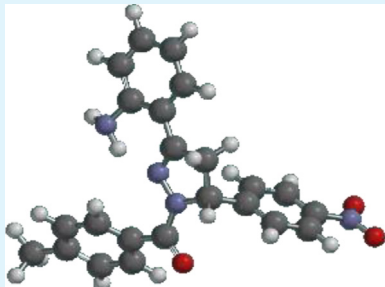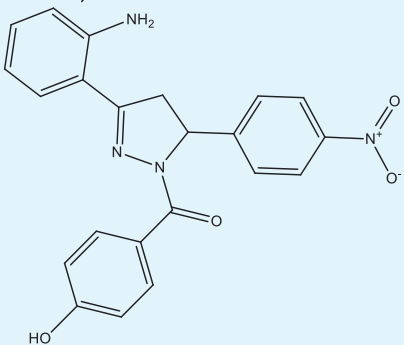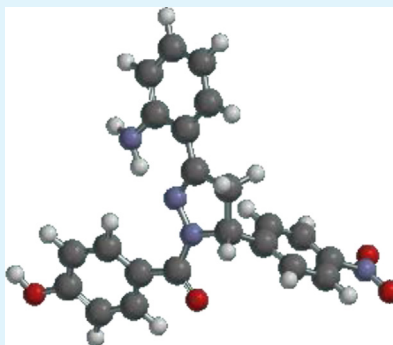
**Table 1: Schematic structures of the modeled compounds; Ma\* = compound from.[28]**
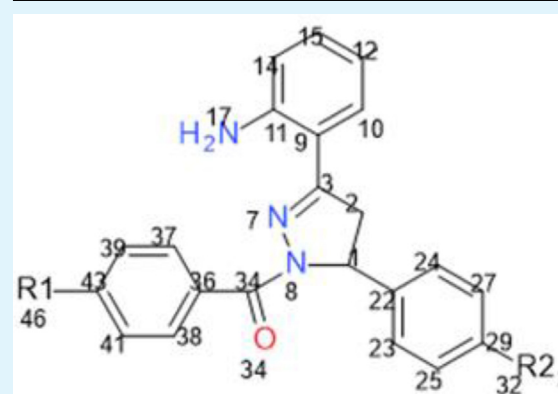


| Compound | R1 | R2 | Name |
|---|---|---|---|
| **M1** | F | NO₂ | [3-(2-aminophenyl)-5-(4-nitrophenyl)-4,5-dihydro-1*H*-pyrazol-1-yl](4-fluorophenyl)methanone |
| **M2** | NO₂ | F | [3-(2-aminophenyl)-5-(4-fluorophenyl)-4,5-dihydro-1*H*-pyrazol-1-yl](4-nitrophenyl)methanone |
| **M3** | CH₃ | NO₂ | [3-(2-aminophenyl)-5-(4-nitrophenyl)-4,5-dihydro-1*H*-pyrazol-1-yl](4-methylphenyl)methanone |
| **M4** | OH | NO₂ | [3-(2-aminophenyl)-5-(4-nitrophenyl)-4,5-dihydro-1*H*-pyrazol-1-yl](4-hydroxyphenyl)methanone |
| **M5** | OCH₃ | NO₂ | [3-(2-aminophenyl)-5-(4-nitrophenyl)-4,5-dihydro-1*H*-pyrazol-1-yl](4-methoxyphenyl)methanone |
| **M6** | NO₂ | NO₂ | [3-(2-aminophenyl)-5-(4-nitrophenyl)-4,5-dihydro-1*H*-pyrazol-1-yl](4-nitrophenyl)methanone |
| **Ma** | F | CN | 4-[3-(2-amino-3,5-dibromophenyl)-1-(4-fluorobenzoyl)-4,5-dihydro-1*H*-pyrazol-5-yl]benzonitrile |

for **M1**, 1.490 Å for **M2**, 1.490 Å for **M3**, 1.479 Å for **M4**, 1.481 Å for **M5**, 1.486 Å for **M6** and 1.487 Å for **Ma**. The N−N bond length in the pyrazole ring was calculated to be 1.376 Å for M1, 1.378 Å for M2, 1.372 Å for **M3**, 1.376 Å for **M4**, 1.375 Å for **M5**, 1.381 Å for **M6** and 1.374 Å for **Ma**; these values have been experimentally found to be 1.385 and 1.369 Å,[40] and 1.3827 Å[27] for similar compounds. In

**Table 2: Optimized structures of M1−M6 in 2-D and 3-D.**

| Compound | 2-D structure | 3-D structure |
|---|---|---|
| M1 |  |  |
| M2 |  |  |
| M3 |  |  |
| M4 |  |  |

**Table 2** (*continued*)

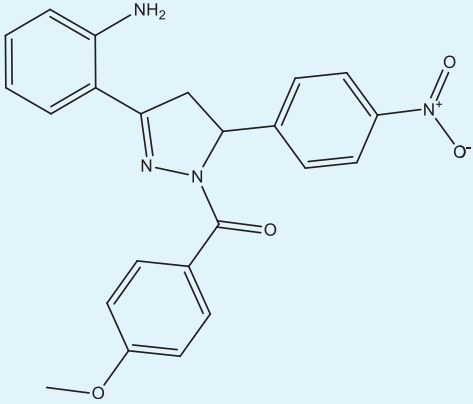| Compound | 2-D structure | 3-D structure |
|---|---|---|
| **M5** |  |  |
| **M6** |  |  |

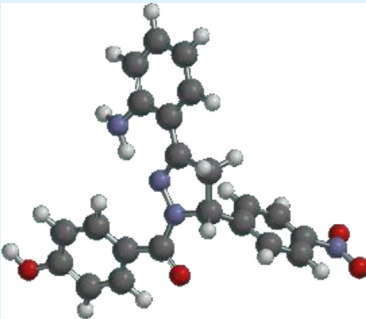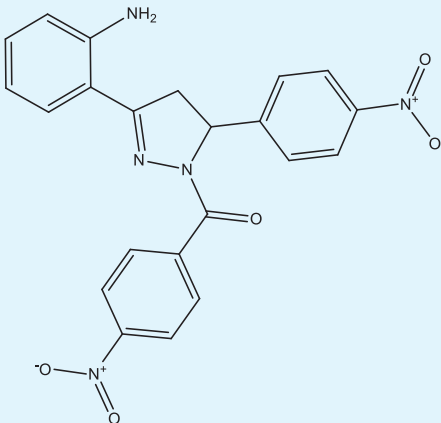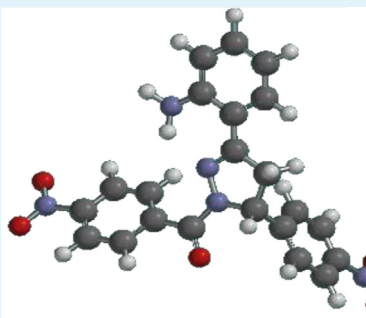addition, The N8−C34 bond length value was 1.383 Å for **M1**, 1.378 Å for **M2**, 1.381 Å for **M3**, 1.360 Å for **M4**, 1.380 Å for **M5**, 1.380 Å for **M6** and 1.374 Å for **Ma**.

The C2−C3−N7 bond angle for the six compounds was calculated to be 112.22°, 112.6°, 112.23°, 112.17°, 112.15° and 112.63° for **M1**−**M6**, respectively. However, N7−N8−C3 was 109.66° for **M1**, 109.65° for **M2**, 109.48° for C3, 109.55° for **M4**, 109.74° for **M5** and 109.67° for **M6**. These two bond angles indicated that the pyrazole ring was distorted from planarity by the aryl and benzoyl rings, as reflected in the dihedral angles (Table 3), thus revealing that aryl and benzoyl groups have more profound effects on the pyrazole ring than the extended R1 and R2 substituents.

*Frontier molecular orbital and UV−vis absorption properties*

The frontier orbital energies, such as the highest occupied molecular orbital energy (HOMO), lowest unoccupied molecular orbital (LUMO) and band gaps, are critical parameters for kinetic and thermodynamic stability studies, and prediction of reactivity and photochemical properties.[41−46] The frontier orbital molecular overlay revealed that the HOMO overlay was essentially on ring, extending over the two nitrogen atoms of the pyrazole ring, whereas the LUMO overlay was on the phenyl ring for **M1, M3, M4** and **M5**, and was on the benzoyl ring for **M1** and **M6**

(Figure 1). The calculated frontier molecular orbitals LUMO, HOMO and HOMO−LUMO (ΔEg) were, respectively, −2.50, −5.92 and 3.42 eV for **M1**; −2.77, −5.91 and 3.14 eV for **M2**; −2.85, −5.87 and 3.02 eV for **M3**; −2.43, −5.86 and 3.43 eV for **M4**; −2.42, −5.86 and 3.37 eV for **M5**; −2.90, −6.06 and 3.16 eV for **M6**; and −2.26, −6.10 and 3.83 for **Ma**. The replacement of a cyano group in **Ma** with $NO_2$ as in **M1** led to a decrease in LUMO energy with an increase in HOMO energy, thus resulting in a decrease in ΔEg by 0.41 eV and profound effects on the electron withdrawing capacity of $NO_2$ compared with the CN group. The interchanged **M1** F and $NO_2$ positions in **M2** further decreased the ΔEg by 0.28 eV with respect to **M1**, thus indicating that the amide group enhanced the electron withdrawing ability of $NO_2$. **M3, M4, M5** and **M6** were modeled by the replacement of fluorine in **M1** with $CH_3$, OH, $OCH_3$ and $NO_2$, respectively. **M3, M5** and **M6** presented ΔEg than **M1**; however, **M6** showed the lowest ΔEg because of lowering of the LUMO energy (−2.90 eV) and stabilization of the HOMO, thereby decreasing the π-electron density of the aromatic rings. Thus, **M6** was expected to be relatively more reactive toward nucleophiles (Table 2).

Other calculated reactivity descriptors such as chemical hardness (η), chemical potential (μ) and global electrophilicity (ω) were, respectively, 1.71, −4.21 and 5.182 eV for **M1**; 1.57, −4.34 and 5.998 eV for **M2**; 1.51, −4.36 and 6.295 eV

**Table 3: Selected bond length, bond angle and dihedral angle for the studied compounds.**

| Bond length(Å) | M1 | M2 | M3 | M4 | M5 | M6 | Ma |
|---|---|---|---|---|---|---|---|
| C1−C2 | 1.552 | 1.550 | 1.547 | 1.551 | 1.552 | 1.550 | 1.546 |
| C1−N8 | 1.482 | 1.490 | 1.490 | 1.479 | 1.481 | 1.486 | 1.487 |
| C2−C3 | 1.523 | 1.520 | 1.522 | 1.522 | 1.523 | 1.522 | 1.522 |
| C3−N7 | 1.299 | 1.298 | 1.300 | 1.299 | 1.299 | 1.298 | 1.295 |
| N7−N8 | 1.376 | 1.378 | 1.372 | 1.376 | 1.375 | 1.381 | 1.374 |
| C3−C9 | 1.457 | 1.458 | 1.457 | 1.450 | 1.457 | 1.457 | 1.457 |
| N8−C34 | 1.383 | 1.378 | 1.381 | 1.360 | 1.386 | 1.380 | 1.381 |
| C34−O35 | 1.228 | 1.228 | 1.235 | 1.221 | 1.229 | 1.227 | 1.223 |
| C11−N17 | 1.358 | 1.357 | 1.36 | 1.359 | 1.357 | 1.357 | 1.358 |
| C14−Br20 | 1.92 | 1.919 | 1.92 | 1.924 | 1.921 | 1.919 | 1.921 |
| C12−Br21 | 1.916 | 1.917 | 1.914 | 1.914 | 1.918 | 1.913 | 1.914 |
| C29−C32 | 1.471 | 1.348 | 1.466 | 1.471 | 1.471 | 1.472 | 1.430 |
| C32−N33 | 1.231 | − | 1.231 | 1.231 | 1.231 | 1.230 | 1.155 |
| C43-X46 | 1.346 | 1.474 | 1.498 | 1.361 | 1.359 | 1.474 | 1.389 |
| Bond angle (°) | | | | | | | |
| C1−C2−C3 | 102.65 | 103.26 | 102.71 | 102.41 | 102.56 | 103.11 | 102.80 |
| C2−C3−N7 | 112.22 | 112.6 | 112.23 | 112.17 | 112.15 | 112.63 | 112.15 |
| C3−N7−N8 | 109.66 | 109.65 | 109.48 | 109.55 | 109.74 | 109.67 | 109.73 |
| N8−C34−C36 | 119.93 | 119.14 | 102.67 | 120.37 | 119.1 | 119.2 | 120.22 |
| Dihedral angle (°) | | | | | | | |
| C11−C9−C3−N7 | −0.64 | 0.30 | −2.42 | −3.53 | −0.72 | 1.85 | −2.94 |
| C10−C9−C3−C2 | 0.30 | 0.35 | −0.77 | −2.30 | 0.26 | 1.91 | −2.09 |
| C2−C1−C22−C24 | 111.01 | −52.34 | −41.6 | −71.79 | −110.87 | −57.52 | −73.11 |
| N8−C1−C22−C23 | 47.07 | 62.37 | −92.22 | −140.77 | 46.92 | −123.25 | −112.47 |
| C1−N8−C34−035 | −1.37 | 1.16 | −0.61 | −3.23 | −1.30 | −0.47 | −2.35 |
| C38−C36−C34−O35 | −30.08 | 30.81 | −10.79 | −25.60 | −29.55 | 29.72 | −29.56 |

Ma = Experimental data of the compound from Ref.[28].

for **M3**; 1.72, −4.15, and 5.009 eV for **M4**;1.69, −4.12 and 5.00 eV for **M5**; and 1.58, −4.48 and 6.351 eV for **M6**. The μ and ω values for **M6** further indicated that the compound would be a good electron acceptor with strong electron pulling effects toward the two NO$_2$ groups. This finding was in agreement with the effect of the NO$_2$ group observed on 4-(3-(2-amino-3,5-dibromophenyl)-1-(4-nitrobenzoyl)-4,5-dihydro-1*H*-pyrazol-5-yl)benzonitrile by Santhi and Bharathi.[28] The electron donating power (ω$^−$) and electron accepting power (ω$^+$) describe the tendency of a molecule to release electrons and to accept electrons, respectively; a smaller ω$^−$ indicates a better donor of electron density, and a greater ω$^+$ indicates better accepting electron capacity. The values for ω$^−$ demonstrated that **M1, M4** and **M5** were good electron donors, whereas ω$^+$ indicated the tendency of **M2, M3** and **M5** to be good electron acceptors, in line with the μ and ω values (Table 4).

The absorption peaks, oscillator strength and percentage of the molecular orbitals involved in transitions, calculated for **M1−M6** at B3LYP/6-31G (p,d), are displayed in Table 5. The transition probability, as measured by oscillator strength (OS), corresponded to the fraction of negative charges (electrons) that accomplished a given transition. OS values <0.005 were considered to indicate transitions emanating from low absorption bands in the studied compounds; thus, only transitions with OS > 0.005 were considered in this study. **M1** showed four strong absorptions, at 304.69, 333.69, 349.07 and 408.24 nm, arising from HOMO-2 → LUMO (94%), HOMO-1 → LUMO (96%), HOMO → LUMO + 1 (89%) and HOMO → LUMO (98%), respectively; the longest λ$_{max}$ was characterized as a π−π* transition arising from HOMO →

LUMO. For **M2**, five strong absorption peaks were identified, at 305.98, 337.57, 341.62, 356.73 and 453.95 nm, with an OS of 0.0463, 0.0081, 0.2840, 0.0359 and 0.0285, respectively. The molecular orbitals' percentage contributions to these transitions were as follows: HOMO-3 → LUMO (42%) and HOMO-4 → LUMO (35%) for 305.98 nm; HOMO-2 → LUMO (87%) for 337.57 nm; HOMO → LUMO+1 86% for 342 nm; HOMO-2 → LUMO 99% for 358 nm; and HOMO → LUMO 99% for 453.95 nm.

In addition, **M3** showed five strong absorption peaks, with HOMO-2 → LUMO (81%) for 408.96 nm; HOMO-5 → LUMO (67%) for 420.81 nm; HOMO-2 → LUMO+1 (44%) and HOMO-1 → LUMO +1 (33%) for 426.26 nm; HOMO-1 → LUMO+1 (45%) and HOMO → LUMO+1 (38%) for 439.54 nm; HOMO-1 → LUMO (88%) for 445.90 nm; and HOMO → LUMO (96%) for 494.49 nm, arising from a low absorption band of 0.0059 OS. For **M4**, 309.69, 332.48, 347.16 and 409.31 nm were the four absorption peaks with OS higher than 0.005, arising from HOMO-1 → LUMO+1 (94%), HOMO-2 → LUMO (92%), HOMO → LUMO+1 (86%) and HOMO → LUMO (98%), respectively. Likewise, 313.41, 337.82, 347.01, 351.47 and 417.91 nm were five absorption peaks with OS higher than 0.005 arising from HOMO-1 → LUMO+1 (96%), HOMO-2 → LUMO (92%), HOMO → LUMO+1 (79%), HOMO-1 → LUMO (93%) and HOMO → LUMO (98%), respectively, for **M5**. The 417.91 nm absorption peak with the highest OS value was characterized as a π−π* transition. For **M6**, five strong absorption peaks at 329.32, 342.96, 349.68, 407.32 and 451.04 nm were identified with OS values of 0.0199, 0.2651, 0.0460, 0.0125 and 0.0267, respectively: HOMO-1 → LUMO+1 (97%) for 329 nm;
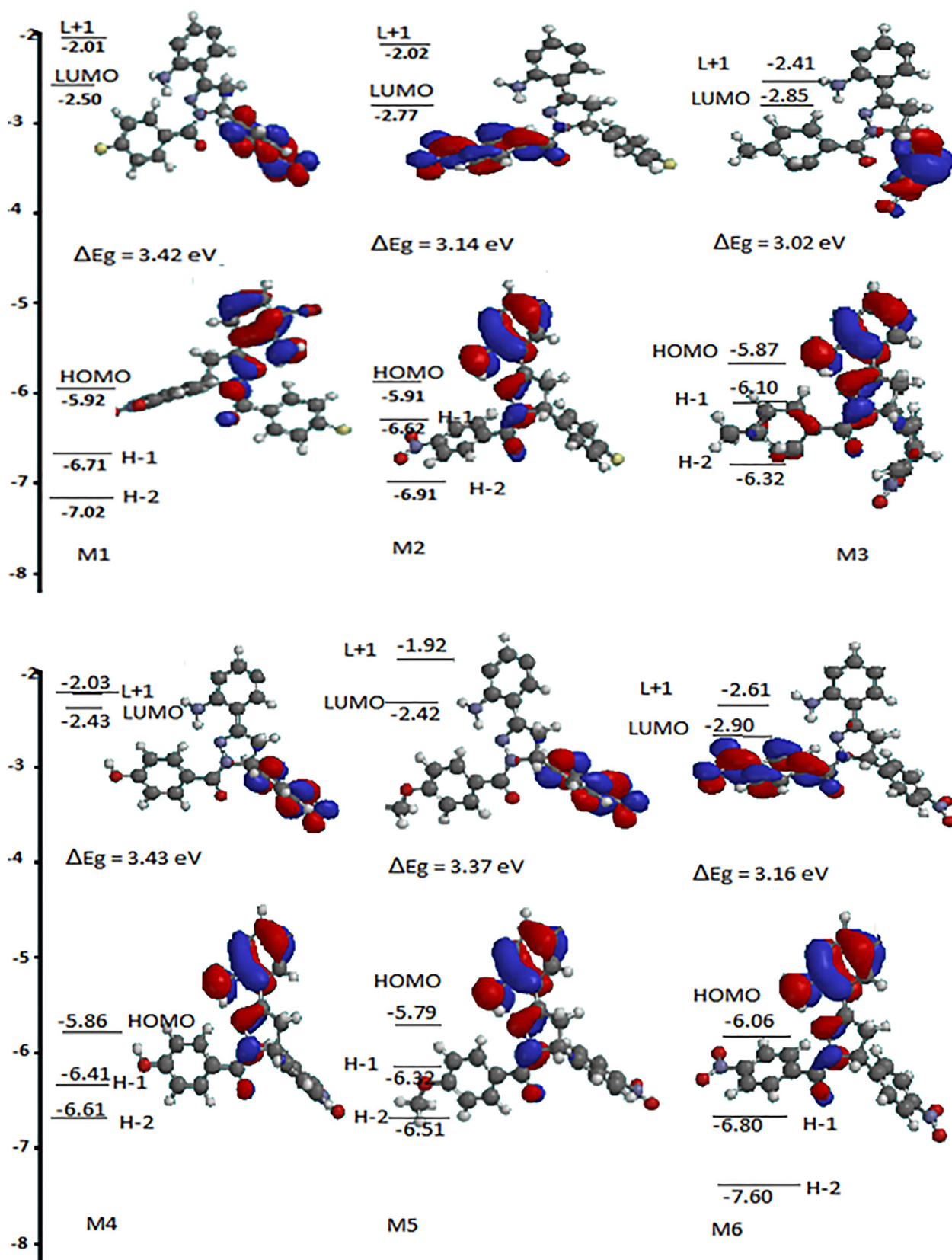
**Figure 1:** Frontier molecular orbitals for compounds **M1–M6**.

**Table 4: Molecular orbitals and reactivity indices.**

| Parameter | M1 | M2 | M3 | M4 | M5 | M6 | Ma |
|---|---|---|---|---|---|---|---|
| HOMO (eV) | −5.92 | −5.91 | −5.87 | −5.86 | −5.79 | −6.06 | −6.10 |
| LUMO (eV) | −2.50 | −2.77 | −2.85 | −2.43 | −2.42 | −2.90 | −2.26 |
| HOMO−1 (eV) | −6.71 | −6.62 | −6.10 | −6.41 | −6.32 | −6.90 | −6.79 |
| HOMO−2 (eV) | −7.02 | −6.91 | −6,32 | −6.61 | −6.51 | −7.60 | −7.21 |
| LUMO+1 (eV) | −2.01 | −2.02 | 2.41 | −2.03 | −1.92 | −2.61 | −1.78 |
| $\Delta E_g$ (eV) | 3.42 | 3.14 | 3.02 | 3.43 | 3.37 | 3.16 | 3.83 |
| $\eta$ (eV) | 1.71 | 1.57 | 1.51 | 1.715 | 1.685 | 1.58 | 1.92 |
| $\mu$ (eV) | −4.21 | −4.34 | −4.36 | −4.145 | −4.105 | −4.48 | −4.18 |
| $\chi$ (eV) | 4.21 | 4.34 | 4.36 | 4.145 | 4.105 | 4.48 | 4.18 |
| $\omega$ (eV) | 5.182 | 5.998 | 6.295 | 5.009 | 5.00 | 6.351 | 4.562 |
| $\omega+$ (eV) | 3.291 | 4.025 | 4.303 | 3.151 | 3.158 | 4.309 | 2.700 |
| $\omega-$ (eV) | 7.501 | 8.365 | 8.663 | 7.296 | 7.263 | 8.789 | 6.880 |
| $\sigma$ (eV$^{-1}$) | 0.855 | 0.785 | 0.755 | 0.8575 | 0.8425 | 0.7900 | 0.5208 |
| $\Delta E_n$ (eV) | 1.827 | 2.444 | 2.670 | 1.722 | 1.7378 | 2.661 | 1.334 |
| $\Delta E_e$ (eV) | 10.247 | 11.124 | 11.410 | 10.011 | 9.948 | 11.621 | 9.715 |

Ma = Theoretical data of the compound from Ref.[28].

HOMO → LUMO+2 (89%) for 324.9 nm; HOMO-1 → LUMO (99%) for 349.68 nm; HOMO → LUMO+1 (99%) for 407 nm; and HOMO → LUMO (99%) for 451 nm. The absorption peak with the highest OS was characterized as a π−π* transition, and the absorption peak next to the highest OS was characterized as an n−π* transition. All the compounds had one or two triplet transitions, thus potentially indicating that they possessed both orbital unpaired and spin unpaired electrons. Consequently, singlet transitions with sufficiently long lifetimes might have led to de-inversion of the spin of some of the electrons, thus generating a triplet.

*Molecular electrostatic potential analysis*

The static distribution of charge density is associated with the electrostatic potential map (MEP) distribution of charge on a molecule, and is a useful parameter for analyzing and predicting the responsiveness of a molecule toward an incoming electrophile or nucleophile during reaction initiation.[47] This parameter has been successfully used to explain stacking and self-assembly of polymeric molecules and dyes, and the orientation of molecules in three-dimensional crystals.[48] The MEP was simulated according to the optimized geometry obtained from DFT calculation to predict electrophilic and nucleophilic sites of attack. In Figure 2, blue indicates a positive region indicating electrophilic centers/electron-deficient areas; red represents the negative regions (areas with excess electrons) for nucleophilic reactivity/electron-rich centers of a molecule; and green represents regions with essentially zero potential.[49−51] Generally, the MEP ranged from red to orange to yellow to green to blue (Figure 1). The negative (red) regions were located at the carbonyl oxygen and cyano group, thus indicating the most probable sites for electrophilic attack. The regions with excess electrons could result in intermolecular pulling of positive regions of nearby molecules, thus distorting the π−π stacking arrangement of these molecules.

*Vibration frequencies*

Vibration frequency is a powerful and effective technique for identification of the organic functional groups of organic compounds; it can distinguish a molecular conformer form either its tautomer or isomer. Comparison of experimental and calculated vibrational modes with appropriate functional group assignment provides meaningful and useful information for understanding fairly complex systems.[34] In addition, when experimental data are not available, the theoretical calculated vibration frequencies can be used with a reasonable level of accuracy to understand the effects of functional groups on molecules. Scaling of the calculated wave numbers increases the reliability and utility of the calculated frequency[28,52]; thus, a 0.9608 scaling factor was used in this work. The DFT-B3LYP/6-31G(d,p) level of calculation was used to determine the vibration frequencies of M1−M6 compounds, and the results were compared with those of 4-(3-(2-amino-3,5-dibromophenyl)-1-(benzoyl)-4,5-dihydro-1*H*-pyrazol-5-yl)benzonitriles.[28] The scaled and unscaled vibration frequencies calculated with the DFT method are shown in Table 6. The calculated symmetric and asymmetric N−H stretching vibrations were 3394 and 3551 cm$^{-1}$ for M1; 3399 and 3552 cm$^{-1}$ for M2; 3385 and 3542 cm$^{-1}$ for M3; 3389 and 3549 cm$^{-1}$ for M4; 3391 and 3551 cm$^{-1}$ for M5; and 3399 and 3551 cm$^{-1}$ for M6. The value has been experimentally observed to be 3433 cm$^{-1}$ and calculated to be 3452 cm$^{-1}$ for Ma.[28] Experimental observations have been conducted at 3390, 3378 and 3360 cm$^{-1}$ in 1-((1,3-diphenyl-1*H*-pyrazol-4-yl)methylene)-4-phenylsemicarbazide, 4-phenyl-1-((1-phenyl-3-p-tolyl-1*H*-pyrazol-4-yl)methylene)semicarbazide and 1-((3-(4-hydroxyphenyl)-1-phenyl-1*H*-pyrazol-4-yl)methylene)-4-phenylsemicarbazide, respectively.[8] The impure in plane bending N−H vibration (βN-H) was blended with vC = C stretching, as shown in Table 6; thus, the βN-H was calculated to be 1345, 1394, 1349, 1344, 1346 and 1345 cm$^{-1}$ for M1−M6, respectively, but has been reported to be 1398 and 1402 cm$^{-1}$ for Ma.[28]

The aromatic C−H stretching vibrations for the compound were in the range of 3250−3102 cm$^{-1}$, but were scaled to be in the region 2984−2978 cm$^{-1}$. The C−H asymmetric stretching vibration for compounds M1−M6 was calculated to be 3112, 3195, 3070, 3107, 3106 and 3104 cm$^{-1}$; the asymmetric C−H symmetric vibrations were 2988, 2980, 2978, 2984, 2991 and 2984 cm$^{-1}$ for M1−M6, respectively.

**Table 5: Calculated absorption peaks, oscillation strength and molecular orbitals involved in transitions for M1−M6.**

| $\lambda_{max}$ (nm) | Oscillation strength | MO involved in transitions |
|---|---|---|
| **M1** | | |
| 304.60 | 0.0349 | HOMO-2 → LUMO 94% |
| 333.69 | 0.0125 | HOMO-1 → LUMO 96% |
| 349.07 | 0.2918 | HOMO → LUMO+1 89% |
| 408.24 | 0.0105 | HOMO → LUMO 98% triplet |
| **M2** | | |
| 305.98 | 0.0463 | HOMO-3 → LUMO 42% |
| | | HOMO-4 → LUMO 35% |
| 337.57 | 0.0081 | HOMO-2 → LUMO 87% |
| 341.62 | 0.2840 | HOMO → LUMO+1 86% |
| 356.73 | 0.0359 | HOMO-1 → LUMO 99% |
| 453.97 | 0.0285 | HOMO → LUMO 99% triplet |
| **M3** | | |
| 408.96 | 0.0131 | HOMO-2 → LUMO 81% |
| 420.81 | 0.0177 | HOMO-5 → LUMO 67% |
| 426.26 | 0.0243 | HOMO → LUMO+1 44% |
| | | HOMO-1 → LUMO+1 33% |
| 439.54 | 0.0394 | HOMO-1 → LUMO+1 45% |
| | | HOMO → LUMO+1 38% |
| 445.90 | 0.0082 | HOMO-1 → LUMO 88% |
| 494.49 | 0.0059 | HOMO → LUMO 96% triplet |
| **M4** | | |
| 309.69 | 0.0983 | HOMO-1 → LUMO+1 94% |
| 332.48 | 0.0142 | HOMO-2 → LUMO 92% |
| 341.18 | 0.0057 | HOMO-1 → LUMO 95% |
| 347.16 | 0.3138 | HOMO → LUMO+1 86% |
| 409.31 | 0.0109 | HOMO → LUMO 98% triplet |
| **M5** | | |
| 313.41 | 0.0901 | HOMO-1 → LUMO+1 96% |
| 337.82 | 0.0253 | HOMO-2 → LUMO 92% |
| 347.01 | 0.2753 | HOMO → LUMO+1 79% |
| 351.40 | 0.0416 | HOMO-1 → LUMO 93% |
| 417.91 | 0.0115 | HOMO → LUMO 98% triplet |
| **M6** | | |
| 329.32 | 0.0199 | HOMO-1 → LUMO+1 97% |
| 342.96 | 0.2651 | HOMO → LUMO+2 89% |
| 349.68 | 0.0460 | HOMO-1 → LUMO 99% |
| 407.32 | 0.0125 | HOMO → LUMO+1 99% triplet |
| 451.04 | 0.0267 | HOMO → LUMO 99% triplet |

The C−H in-plane bending (βC-H) vibrations were 1145, 1131 and 1127 cm$^{-1}$ for **M1**; 1165, 1142 and 1130 cm$^{-1}$ for **M2**; 1150, 1143 and 1132 cm$^{-1}$ for **M3**; 1156, 1141 and 1130 cm$^{-1}$ for **M4**; 1154, 1137 and 1125 cm$^{-1}$ for **M5**; and 1155, 1137 and 1131 cm$^{-1}$ for **M6**. The βC-H vibration for 4-(3-(2-amino-3,5-dibromophenyl)-1-(benzoyl)-4,5-dihydro-1*H*-pyrazol-5-yl)benzonitriles has been experimentally observed at 1165 cm$^{-1}$ and calculated to be 1175 cm$^{-1}$.[28] The C−H out-of-plane (τC-H) vibrations appeared in the region of 959−851 cm$^{-1}$ for **M1**; 952−809 cm$^{-1}$ for **M2**; 957−822 cm$^{-1}$ for **M3**; 928−790 cm$^{-1}$ for **M4**; 941−860 cm$^{-1}$ for **M5**; and 959−855 cm$^{-1}$ for **M6**.

The C = O stretching vibrations appeared in the region of 1655 cm$^{-1}$ for **M1**; 1662 cm$^{-1}$ for **M2**; 1620 cm$^{-1}$ for **M3**; 1653 cm$^{-1}$ for **M4**; 1657 cm$^{-1}$ for **M5**; and 1663 cm$^{-1}$ for **M6**. These vibrations have been observed at 1662 cm$^{-1}$ for *N*-[(4-chlorophenyl)]-4-oxo-4-[oxy] butane amide,[53] 1637 cm$^{-1}$ for diethyl 1*H*-pyrazole-3,5-dicarboxylate,[25]

1660 cm$^{-1}$,[28] 1701 cm$^{-1}$ for 4-chloro-3,5-dimethyl-1*H*-pyrazol-1-yl) (p-tolyl) methanone[26] and 1683 cm$^{-1}$ for 4-phenyl-1-((1-phenyl-3-p-tolyl-1*H*-pyrazol-4-yl)methylene)semicarbazide.[8] The calculated vC-NO$_2$ stretching was 1337 cm$^{-1}$ for **M3** but was 1342 cm$^{-1}$ for other compounds. The vNO$_2$ (acceptor group) stretching was calculated to be 1605, 1603, 1567, 1605 and 1605 cm$^{-1}$ for **M1−M5**, respectively; meanwhile, M6 showed three vibrational modes for vNO$_2$, at 1604, 1556 and 1553 cm$^{-1}$. However, these bands were calculated for *N*-methyl-*N*-(2,4,6-trinitrophenyl) nitramide to be in the region of 1633−1591 cm$^{-1}$ and 1388−1348 cm$^{-1}$, and were assigned to vNO$_2$ asymmetric and symmetric stretching vibrations, respectively.[54] The vNH$_2$ group (electron donor) stretching was 1560 cm$^{-1}$ for **M1** and **M3**; 1559 cm$^{-1}$ for **M2**, **M4** and **M6**; and 1556 cm$^{-1}$ for **M5**. Generally, aromatic compounds containing fluorine show vC−F stretching in the region 1000−1400 cm$^{-1}$.[55] However, compounds **M1** and **M2** showed these vibrations at 1237 cm$^{-1}$ and have been reported at 1223 cm$^{-1}$.[28]

*Polarizability and hyperpolarizability*

The static polarizability (α), hyperpolarizability (β) and electric dipole moment (μ) based on the finite field method were calculated for the six compounds at DFT B3LYP/6-31G(d,p). The total static dipole moment (μ), mean polarizability ($\alpha_o$) and mean first hyperpolarizability ($\beta_0$) were defined by using the x,y,z component, as shown in equations (8)−(14):

$$\mu_{Total} = \left( \mu_x^2 + \mu_y^2 + \mu_z^2 \right)^{1/2} \qquad 8$$

$$\alpha_0 = 1/3 \left( \alpha_{xx} + \alpha_{yy} + \alpha_{zz} \right) \qquad 9$$

$$\alpha^2 = 1/2 \left[ \left( \alpha_{xx} - \alpha_{yy} \right)^2 + \left( \alpha_{zz} - \alpha_{xx} \right)^2 + 6 \left( \alpha_{xx}^2 + \alpha_{yy}^2 + \alpha_{zz}^2 \right) \right] \qquad 10$$

$$\beta_0 = \beta_{Total} = \left( \beta_x^2 + \beta_y^2 + \beta_z^2 \right)^{1/2} \qquad 11$$

$$\beta_x^2 = (\beta xxx + \beta xyy + \beta xzz)^2 \qquad 12$$

$$\beta_y^2 = (\beta yyy + \beta yzz + \beta yxx)^2 \qquad 13$$

$$\beta_z^2 = (\beta zzz + \beta zxx + \beta zyy)^2 \qquad 14$$

The presence of electron donating and electron withdrawing groups on π-conjugated molecules changes the ground state charge distribution and enhances asymmetric polarization of the molecules. Consequently, large nonlinear responses are correlated with a rapid response time; therefore, these molecules are desirable candidates for NLO applications.[56,57] Any molecule with a minimum value of $4.187944 \times 1^{-30}$ esu for the first hyperpolarizability is considered a good candidate for NLO applications.[58] Therefore, these molecules' NLO properties, polarizability and hyperpolarizability were assessed. The dipole moment, an essential parameter explaining the intermolecular
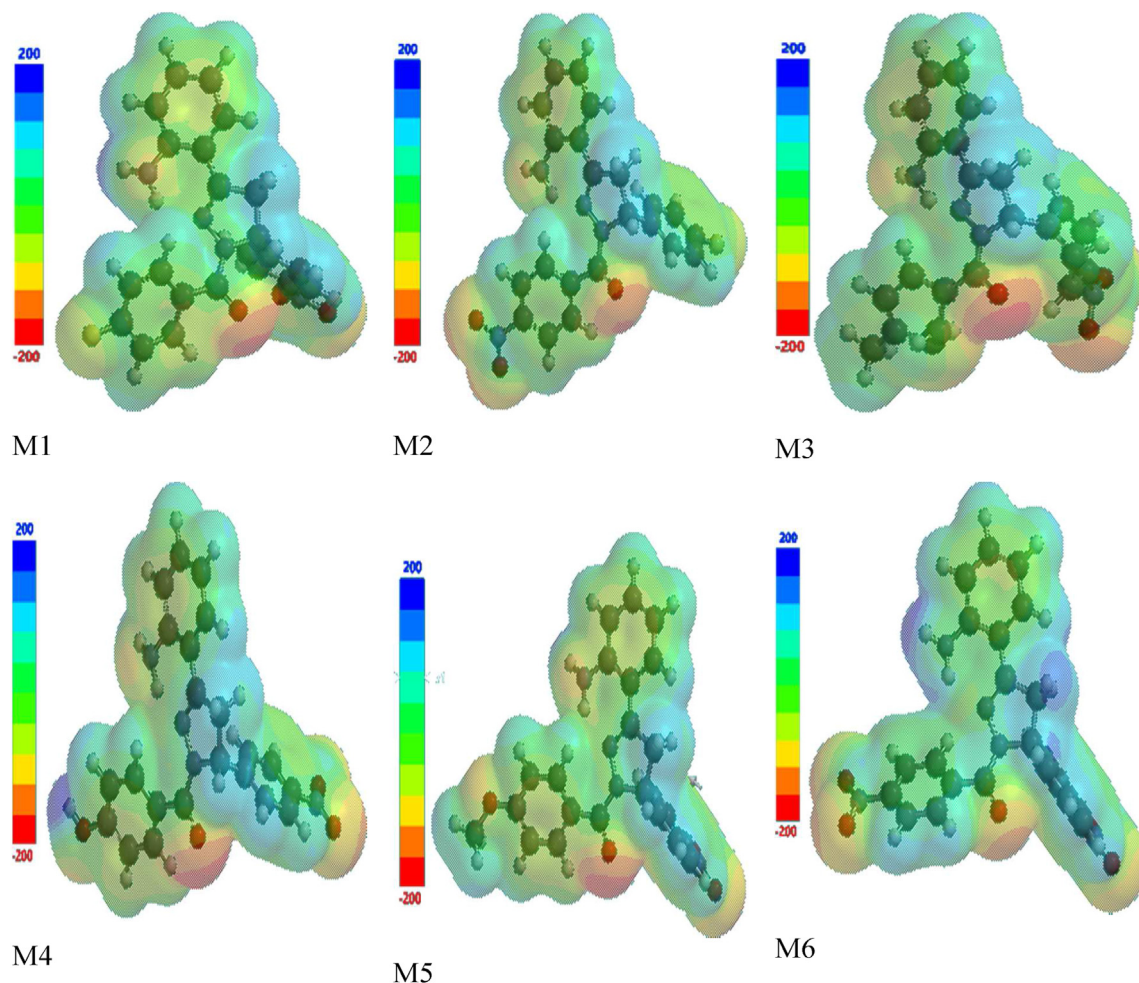
**Figure 2:** Molecular electrostatic potential (MEP) diagram of compounds **M1**–**M6**.

interactions of molecules, is expected to have a higher value with stronger intermolecular interactions. The dipole moment values calculated for **M1**–**M6** were 4.57, 4.06, 5.47, 6.45, 5.32 and 5.14 D (1D = 3.34 × $10^{-34}$ C m), respectively. The $\alpha_o$ calculated for **M1**–**M6** was 3.29, 3.28, 3.26, 3.26, 3.28 and 3.63 × $10^{-23}$ esu, respectively. The $\alpha_o$ for Ma (4-[3-(2-amino-3,5-dibromophenyl)-1-(4-fluorobenzoyl)-4,5-dihydro-1*H*-pyrazol-5-yl]benzonitrile) has been reported to be 3.31 × $10^{-23}$ esu.[28] However, the $\beta_0$ for **M1**–**M6** was 6.04, 5.21, 6.15, 6.74, 6.02 and 7.26 3.31 × $10^{-30}$ esu, respectively, and has been reported to be 8.47 × $10^{-30}$ esu for **Ma**.[28] The $\beta_0$ values for the studied compounds were lower than that of Ma, but approximately 16 times higher than that of urea (0.372 × $10^{-30}$ esu).[57] The model compounds had higher $\beta_0$ values than those of diphenylmethylidene-5-methyl-1*H*-pyrazole-3-carbohydrazide ($\beta_0$ = 2.08 × $10^{-30}$ esu)[59] and diethyl-1-*H*-pyrazole-3,5-dicarboxylate ($\beta_0$ = 1.01 × $10^{-30}$ esu).[24] Interchanging the position of NO$_2$ and F, as shown in **M1** and **M2**, led to a decrease in $\beta_0$ by 0.83 × $10^{-30}$ esu and an increase in absorption wavelength ($\lambda_{max}$) by 75 nm in **M2**. Thus, the position, nature and point of attachment of substituents on the model compound strongly affect the properties of the compound.[57] In addition, **M6** with two NO$_2$ groups increased $\beta_0$; therefore, the presence of an

electron withdrawing group (nitro) on the phenyl ring contributed to higher hyperpolarizability values, possibly because of an inductive effect of the electron withdrawing group on the electronic density in the molecule.[28] Our results showed that **M1**–**M6** compounds may be suitable for NLO applications, and the magnitude of molecular hyperpolarizability was improved by functional group modification (Table 7).

*Molecular docking*

The antihypertensive and antioxidant properties of the studied pyrazole derivatives (**M1**–**M6**) were investigated via molecular docking, and the obtained results were compared with the results for rolipram and taurine. The antihypertensive activity of the compounds was evaluated by considering their inhibitory activity against phosphodiesterases (PDEs). PDEs are enzymes participating in cAMP and cGMP homeostasis by acting on phosphodiester bonds.[60,61] When PDE is inhibited, the cAMP and cGMP levels increase, thereby decreasing calcium levels in cells. Consequently, blood vessels are vasodilated with relaxing of the blood vessels, and the risk of hypertension markedly decreases.[62] However, phosphodiesterase 4 (**PDE4**) has been reported to be the main enzyme in the hydrolysis of

**Table 6: Calculated IR frequencies (cm$^{-1}$) at B3LYP/6-31G(d,p).**

| Assignment | M1 | | M2 | | M3 | | M4 | | M5 | | M6 | | Ma | |
|---|---|---|---|---|---|---|---|---|---|---|---|---|---|---|
| | Unscaled | Scaled | Unscaled | Scaled | Unscaled | Scaled | Unscaled | Scaled | Unscaled | Scaled | Unscaled | Scaled | Expt | Scaled |
| νN-H$_{syn}$ | 3532 | 3394 | 3538 | 3399 | 3523 | 3385 | 3527 | 3389 | 3529 | 3391 | 3538 | 3399 | 3433 | 3452 |
| νN-H$_{Asyn}$ | 3696 | 3551 | 3697 | 3552 | 3687 | 3542 | 3694 | 3549 | 3696 | 3551 | 3696 | 3551 | — | |
| νC-H$_{syn}$ | 3110 | 2988 | 3102 | 2980 | 3099 | 2978 | 3106 | 2984 | 3113 | 2991 | 3106 | 2984 | 2924 | 2980 |
| νC-H$_{Asyn}$ | 3239 | 3112 | 3250 | 3123 | 3195 | 3070 | 3234 | 3107 | 3233 | 3106 | 3231 | 3104 | 3071 | 3104 |
| νC = O | 1723 | 1655 | 1730 | 1662 | 1686 | 1620 | 1720 | 1653 | 1725 | 1657 | 1731 | 1663 | 1655 | 1646 |
| νC = N | 1642 | 1578 | 1637 | 1573 | 1632 | 1568 | 1634 | 1570 | 1634 | 1570 | 1639 | 1575 | 1619 | 1622 |
| νC = C, βN-H | 1345 | 1292 | 1347 | 1294 | 1349 | 1296 | 1344 | 1291 | 1346 | 1293 | 1345 | 1292 | 1398 | 1402 |
| νC = C | 1618 | 1555 | 1614 | 1551 | 1579 | 1517 | 1617 | 1554 | 1618 | 1555 | 1616 | 1553 | 1329 | 1353 |
| βC-H | 1192, 1177, 1172 | 1145, 1131, 1127 | 1213, 1188, 1176 | 1165, 1142, 1130 | 1197, 1189, 1178 | 1150, 1143, 1132 | 1203, 1188, 1176 | 1156, 1141, 1130 | 1201, 1183, 1171 | 1154, 1137, 1125 | 1203, 1183, 1177 | 1155, 1137, 1131 | 1165 | 1175 |
| τC-H | 998 920, 886 | 959, 884, 851 | 991, 948, 843 | 952, 910, 809 | 996, 952 856, | 957, 915, 822 | 966, 956, 886 | 928, 918, 790 | 979, 964, 895 | 941, 926, 860 | 998, 964, 890 | 959, 926, 855 | 987 | 980 |
| νC-F | 1287 | 1237 | 1287 | 1237 | — | — | — | — | — | — | — | — | 1223 | — |
| νC-NO$_2$ | 1397 | 1342 | 1397 | 1342 | 1392 | 1337 | 1397 | 1342 | 1397 | 1342 | 1397 | 1342 | 1450a, 1394a | 1489a, 1397a |
| νNO$_2$ | 1671 | 1605 | 1668 | 1603 | 1631 | 1567 | 1671 | 1605 | 1670 | 1605 | 1669, 1619, 1616 | 1604, 1556, 1553 | | |
| νNH$_2$ | 1624 | 1560 | 1623 | 1559 | 1624 | 1560 | 1623 | 1559 | 1820 | 1556 | 1623 | 1559 | | |
| νC-NH$_2$ | 1658 | 1593 | 1662 | 1597 | 1654 | 1589 | 1664 | 1599 | 1663 | 1598 | 1661 | 1596 | | |
| νOH | | | | | | | 3819 | 3669 | | | | | | |

ν = stretching; β = in-plane bending: τ = out-of-plane bending, Sci = scissors; Ma and a = 4-(3-(2-amino-3,5-dibromophenyl)-1-(4-nitrobenzoyl)-4,5-dihydro-1*H*-pyrazol-5-yl)benzonitrile.[28]

**Table 7: Dipole moment, polarizability and hyperpolarizability of M1−M6.**

**Dipole moment**

| Parameter | M1 | M2 | M3 | M4 | M5 | M6 |
|---|---|---|---|---|---|---|
| $\mu_x$ | 3.2717 | 2.4264 | −4.4201 | 4.22 | 1.2246 | −3.7596 |
| $\mu_y$ | −2.0652 | −2.9515 | −2.3989 | −4.2089 | 4.9235 | 1.4025 |
| $\mu_z$ | −2.4399 | 1.3697 | 2.1446 | −2.4754 | 1.5946 | 3.2168 |
| $\mu_{tot}$ | 4.57 | 4.06 | 5.47 | 6.45 | 5.32 | 5.14 |
| **Polarizability/a.u.** | | | | | | |
| $\alpha_{xx}$ | −242.284 | −236.429 | −258.740 | −246.939 | −237.601 | −255.538 |
| $\alpha_{xy}$ | 11.3659 | 14.9274 | −13.1037 | 6.41700 | −31.0350 | −6.7400 |
| $\alpha_{yy}$ | −218.433 | −225.704 | −184.970 | −203.456 | −211.066 | −262.856 |
| $\alpha_{xz}$ | 12.0644 | −4.6114 | 10.8756 | 12.2329 | −4.94560 | 13.6039 |
| $\alpha_{yz}$ | −16.3197 | −2.0474 | 10.8167 | −16.7704 | −25.3816 | 6.80760 |
| $\alpha_{zz}$ | −206.567 | −202.342 | −216.967 | −208.855 | −215.010 | −217.261 |
| $\alpha_{tot}$ | −222.428 | −221.491 | −220.225 | −219.749 | −221.226 | −245.218 |
| $\alpha \times 10^{-23}$ esu | 3.29 | 3.28 | 3.26 | 3.26 | 3.28 | 3.63 |
| **Hyperpolarizability/a.u.** | | | | | | |
| $\beta_{xxx}$ | 415.4398 | 307.9092 | −499.813 | 399.1294 | 296.4138 | −451.768 |
| $\beta_{xxy}$ | −143.263 | −61.1607 | −94.8057 | −99.1944 | 215.4269 | −151.772 |
| $\beta_{xyy}$ | 160.3521 | 223.159 | −36.6282 | 215.598 | 85.0875 | −278.063 |
| $\beta_{yyy}$ | −5.6029 | −50.0772 | −72.1537 | −181.966 | 262.2293 | 244.9397 |
| $\beta_{xxz}$ | −37.1159 | 8.9984 | 42.1252 | −29.5710 | −7.1656 | 55.6498 |
| $\beta_{xyz}$ | 84.942 | −9.2125 | 34.8642 | 81.0249 | 105.6754 | 53.0815 |
| $\beta_{yyz}$ | −31.9896 | 53.7171 | −11.3035 | −51.069 | 27.7063 | 100.8334 |
| $\beta_{xzz}$ | 103.2154 | 62.224 | −149.912 | 109.4585 | 108.3569 | −91.1906 |
| $\beta_{yzz}$ | −4.1993 | 13.766 | −18.9092 | 2.0788 | 18.0156 | −6.0768 |
| $\beta_{zzz}$ | 5.8459 | −20.1728 | −5.7925 | 4.1569 | −6.0768 | −0.3585 |
| $\beta_{tot}$ | 698.9145 | 602.749 | 711.516 | 779.86 | 697.037 | 840.259 |
| $\beta \times 10^{-30}$ esu | 6.04 | 5.21 | 6.15 | 6.74 | 6.02 | 7.26 |

For (α): 1 a.u. = 0.1482 × $10^{-24}$ esu and for (β): 1 a.u. = 8.6393 × $10^{-33}$ esu).

cAMP, another mediator that controls pro-inflammation and anti-inflammation.[61,62] To investigate the PDE inhibitory activity of the compounds, we performed molecular docking of the compounds on PDE4 (**PDB ID: 1RO6**) downloaded from the Protein Data Bank. The downloaded **1RO6** was complexed with the rolipram drug, a selective PDE4 inhibitor that increases the quantity of cAMP in immune and nerve cells[63,64] and compared the docking results.

Antioxidants are common food additives that inhibit cellular damage mainly through their free radical scavenging ability.[64,65] Free radicals are reactive oxygen species produced in the body through various metabolic processes, in phagocytosis, in prostaglandin synthesis and in the cytochrome P-450 system, as a result of exposure to different physiochemical conditions or pathological states.[66] Excessive free radicals in the body lead to a condition known as oxidative stress, which harmfully alters proteins, lipids and DNA, and can initiate the progression of pathologies including immune system deterioration, atherosclerosis and abnormal cell growth leading to nucleofugality cancer.[66] Analysis of pyrazoline derivatives has indicated that they are promising antioxidants.[67−69] Therefore, we examined the model compounds for their antioxidant ability by docking them against a dehydrogenase inhibitor downloaded from the Protein Data Bank (**PDB ID: 5ADH**). Taurine is an antioxidant involved in protection of hepatic tissue by deactivating reactive oxygen species, thereby removing formation of osmoregulation, calcium homeostasis, lipid peroxidation and protein carbonyl formation, detoxification, cytoprotection and neuromodulation.[70−72] Reports have indicated that taurine concentrations are inversely associated with diabetes complications.[73−75] The optimized structures of the model compounds were used for docking simulations. The docking was performed with AutoDock Tool 1.5.6 and AutoDock Vina 1.1.2; proteins were treated; and molecular interactions between receptors and ligands were visualized with Edupymol version 1.7.4.4 and BIOVIA Discovery studio 2019, as previously reported.[76−84] The grid box using AutoDock tool before use of AutoDock Vina for docking calculations was as follows: center (X = 4.834, Y = 15.305, Z = 24.227) and size (X = 64, Y = 52, Z = 74) for **5ADH**, and (X = 32.382, Y = 72.334, Z = 31.711) and size (X = 62, Y = 58, Z = 66) for **1RO6**, with default exhaustiveness (exhaustiveness = 8) for steady docking calculation speed.

A recent study has indicated that molecular docking of pyrazole derivatives such as carboxy pyrazole derivatives with various cancer cells (breast, MCF-7; bone marrow, K-562; and cervix, HeLa),[6] aryl pyrazoles with tyrosinase enzyme,[85] pyrazole-phenyl semicarbazone derivatives with α-glucosidase,[8] imidazole−pyrazole conjugates with α-glucosidase[10] and 4-aryl-N-(5-methyl-1*H*-pyrazol-3-yl)benzamides with *Acinetobacter baumannii* protein[11] was in agreement with experimental observations, and has also detailed the nature of the protein-ligand interactions. The use of molecular docking for in silico screening of bioactivity of heterorganic compounds, as well as drug design and discovery, has become frequent and relevant in pharmacology.

**Table 8: Binding affinity ($\Delta$G) and hydrogen bonding interactions of the 5ADH and 1RO6 receptors with compounds M1−M6.**

| Ligand | 5ADH receptor | | | | 1RO6 receptor | | | |
|---|---|---|---|---|---|---|---|---|
| | Binding affinity $\Delta$G (kcal/mol) | Inhibition constant Ki ($\mu$M) | H-bond with ligands | H-bond distance (Å) | Binding affinity $\Delta$G (kcal/mol) | Inhibition constant Ki ($\mu$M) | H-bond with ligands | H-bond distance (Å) |
| **M1** | −9.0 | 0.25 | ILE'269 | 2.9 | −9.7 | 0.07 | GLU'304 | 3.2 |
| | | | VAL'294 | 2.4 | | | ASP'392 | 3.2 |
| | | | GLY'202 | 2.3 | | | ASP'275 | 3.5 |
| | | | ARG'269 | 2.1 | | | | |
| | | | ILE'368 | 3.3 | | | | |
| **M2** | −9.3 | 0.15 | ILE'269 | 2.7 | −9.2 | 0.17 | SER'282 | 2.7 |
| | | | VAL'203 | 2.5 | | | GLN'417 | 2.4 |
| **M3** | −9.3 | 0.15 | ILE'269 | 2.7 | −9.4 | 0.12 | HIS'234 | 2.2 |
| | | | ARG'47 | 2.4, 2.6 | | | ASN'395 | 2.0 |
| | | | SER'367 | 3.2 | | | GLN'443 | 3.3, 2.0 |
| | | | ILE'368 | 3.2 | | | | |
| | | | GLY'202 | 2.7 | | | | |
| **M4** | −8.8 | 0.35 | ILE'269 | 3.0 | −9.9 | 0.05 | GLU'304 | 3.5 |
| | | | VAL'294 | 2.8 | | | GLN'417 | 2.8 |
| | | | ARG'369 | 2.1 | | | GLY'280 | 2.8 |
| | | | ILE'368 | 2.3 | | | ASP'392 | 3.1 |
| | | | GLY'202 | 2.3 | | | ASP'275 | 3.5 |
| **M5** | −8.8 | 0.35 | ARG'369 | 2.2 | −8.5 | 0.58 | GLU'304 | 2.4 |
| | | | | | | | ASP'275 | 3.5 |
| | | | | | | | HIS'234 | 2.5 |
| **M6** | −8.8 | 0.35 | SER'48 | 2.6 | −8.9 | 0.29 | THR'345 | 3.3 |
| | | | ILE'269 | 2.6 | | | HIS'307 | 2.5 |
| | | | VAL'203 | 2.5 | | | HIS'234 | 2.4 |
| | | | | | | | ASN'395 | 2.4 |
| **Taurine** | −3.7 | | SER 367 | 2.6 | **Rolipram** −8.8 | 0.35 | ASP'392 | 3.6 |
| | | | ARG 369 | 2.4 | | | HIS'234 | 2.1 |
| | | | ARG 47 | 2.3 | | | GLN'443 | 3.3, 2.4, 3.3 |

Therefore, docking serves as a reliable and time saving method for simulation of binding poses of ligand conformations in the active sites of receptors, and calculation of the binding affinity and interactions of protein-ligand complexes.[86]

The binding affinity of the stable ligands docked with dehydrogenase inhibitor (**PDB ID: 5ADH**) ranged from −8.8 to 9.3 kcal/mol: **M1** (−9.0 kcal/mol), **M2** and **M3** (−9.3 kcal/mol) and **M4, M5** and **M6** (−8.8 kcal/mol). Similar binding affinities (−8.3 to −9.5 kcal/mol) have been reported for 1-benzyl-2-phenyl-1*H*-benzimidazole derivatives docked with dehydrogenase (**PDB ID: 5ADH**).[87] The binding affinity calculated for taurine was −3.7 kcal/mol, as shown in Table 8, thus indicating that these compounds may be excellent inhibitors for APO-liver dehydrogenase and thus possess good antioxidant properties. Ligand interactions with the binding pocket of dehydrogenase (**PDB ID: 5ADH**) revealed that ARG 369 and ARG 202 are involved in hydrogen bond interactions with the $NO_2$ group of **M1**; ARG 295 and ARG 47 are involved in a $\pi$-alkyl interaction; Val 294 is involved in a $\pi$-cation interaction, and VAL 203 is involved in $\pi$-sigma interactions with **M1**. The amino acid residues GLY 202, VAL 203 and ILE 269 are involved in hydrogen bond interactions; PRO 295, ARG 47 and PRO 296 are involved in $\pi$-alkyl interactions; VAL 203 is involved in $\pi$-sigma interactions; and CYS 46 is involved in $\pi$-sulfur interactions with **M2**. In addition, GLY 202, VAL 203, ARG 47 and ILE 269 are involved in hydrogen bonding, and ILE

269, VAL 203, GLY 202, PRO 295 and ARG 47 form $\pi$-alkyl interactions with **M3**. PRO 295 and ARG 47 are involved in $\pi$-alkyl interactions; VAL 203 is involved in $\pi$-sigma interactions; ARG 369 and GLY 202 form hydrogen bond interactions, and HIS 51 is involved in $\pi$-cation interactions with **M4**. Amino acid residues ARG 47, PRO 295 and PRO 296 are involved in $\pi$-alkyl interactions; SER 48 and ARG 369 are involved in hydrogen bonding; VAL 203 forms a $\pi$-sigma interaction; and CYS 46 forms $\pi$-sulfur interactions with **M5**. Furthermore, SER 48, VAL 203 and ILE 269 are involved in hydrogen bonding; ARG 47, PRO 295 and PRO 296 form $\pi$-alkyl interactions; and VAL 203 is involved in a $\pi$-sigma interaction with **M6** (Table 8 and Figure 3). Taurine is involved in hydrogen bonding with SER 367, ARG 369 and ARG 47, and also participates in Van der Waals interactions with VAL 203 and CYS 46. Similar binding modes for protein-ligand interactions have been observed for 1-benzyl-2-phenyl-1*H*-benzimidazole derivatives docked with dehydrogenase (**PDB ID: 5ADH**), and ILE 269, VAL 203, GLY 202, PRO 295 and ARG 47 amino acid residues have been found to be involved in the interactions.[87]

The ligand bound at the active site of the **1RO6** receptor (Figure 4) revealed that MET 347 and ILE 410 are involved in alkyl-$\pi$ interactions; PHE 446, PHE 414 and VAL 281 form $\pi$-$\pi$ stacking, amide-$\pi$ stacking and $\pi$-$\pi$ T-stacking interactions; and GLU 413, GLY 280 and GLN 417 form fluorine-$\pi$ interactions with **M1**. Amino acid residues PHE
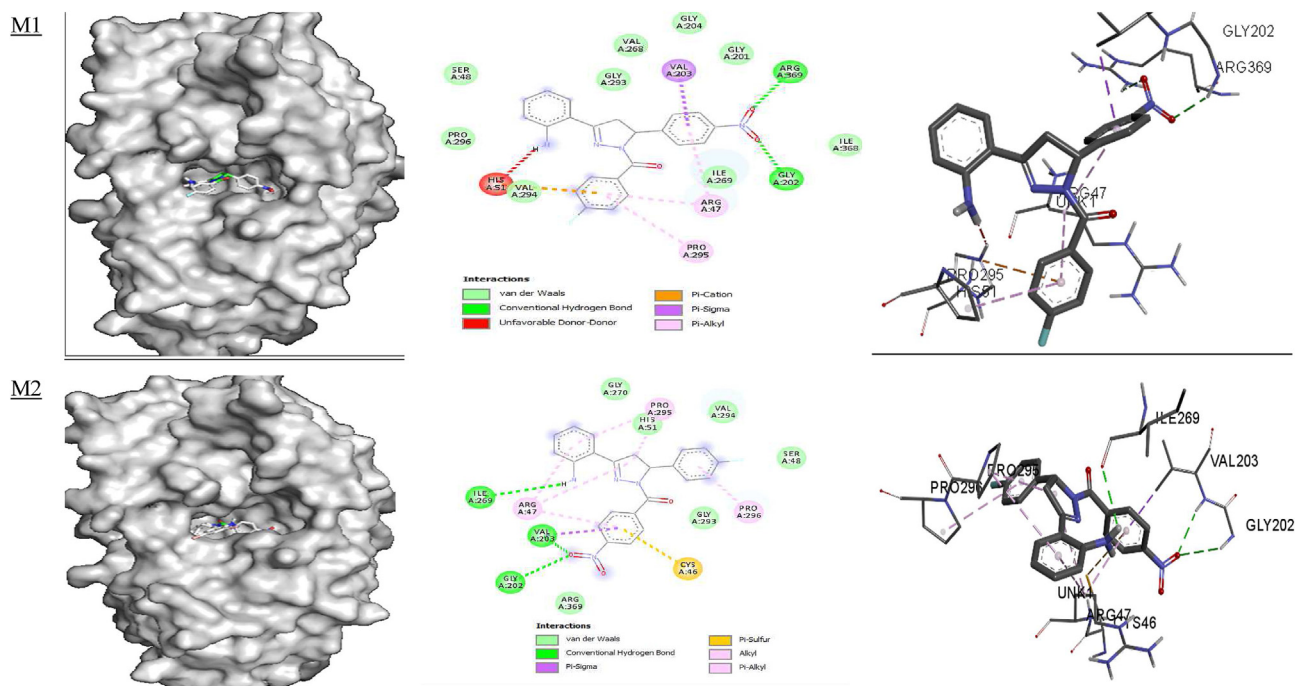
**Figure 3:** Docked complexes of the **5ADH** receptor with compounds **M1−M6**, showing interactions in the binding pocket.
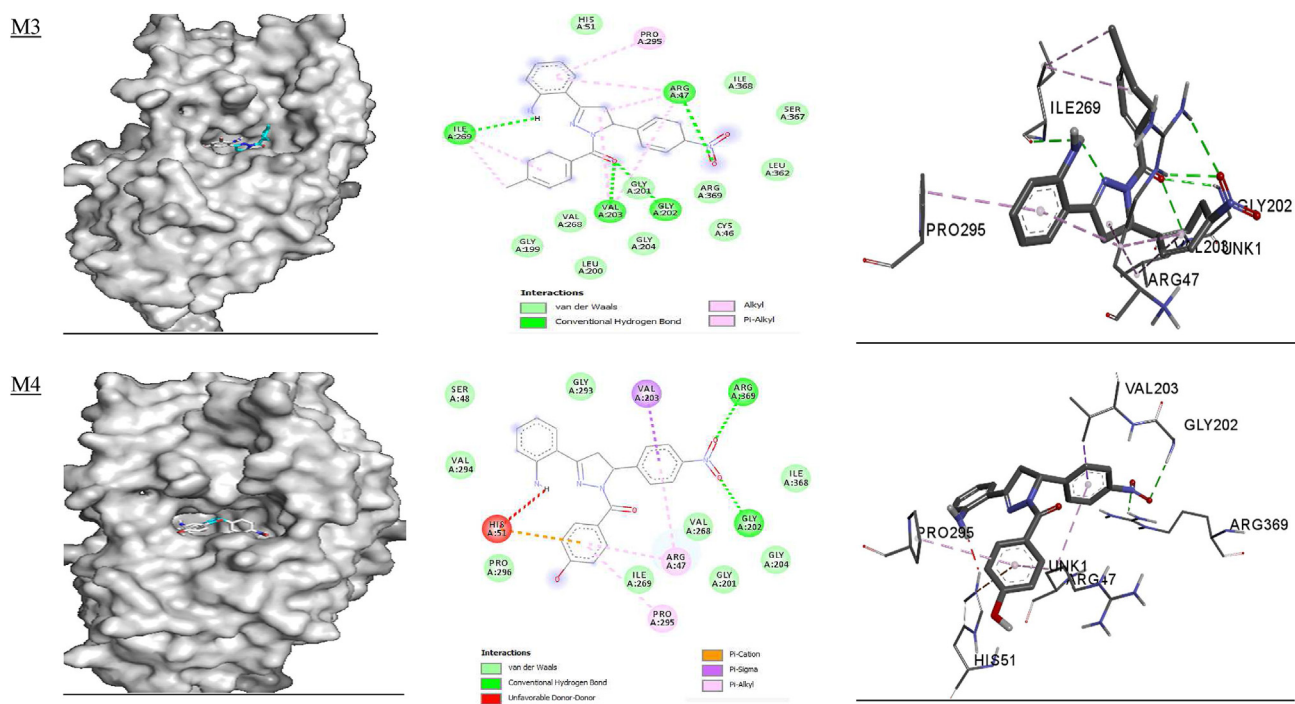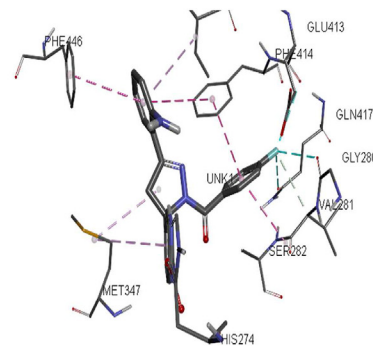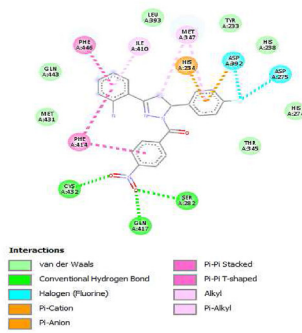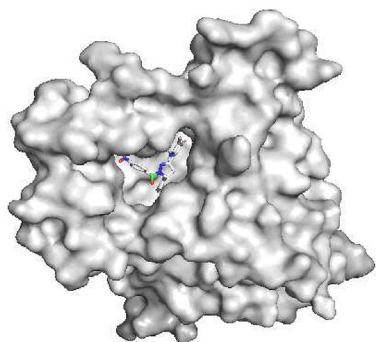


**Figure 3:** continued.

446 and PHE 414 are involved in π-π stacking and form π-π T-stacking interactions; MET 347 and ILE 310 are involved in alkyl-π interactions; CYS 432, SER 282 and GLN 417 participate in hydrogen bonding; ASP 392 and ASP 275 form fluorine-π interactions; and HIS 234 and ASP 392 are involved in π-cationic and anionic interactions with **M2**. In addition, MET 347, PHE 446, ILE 410, TYR 233, LEU 303, HIS 278 and HIS 234 all form alkyl-π interactions, and ASN 395, HIS 234 and GLN 443 are involved in hydrogen bond interactions with **M3**. Amino acids PHE

M5



M6



**Figure 3:** continued.

Tau



**Figure 3:** continued.

M1
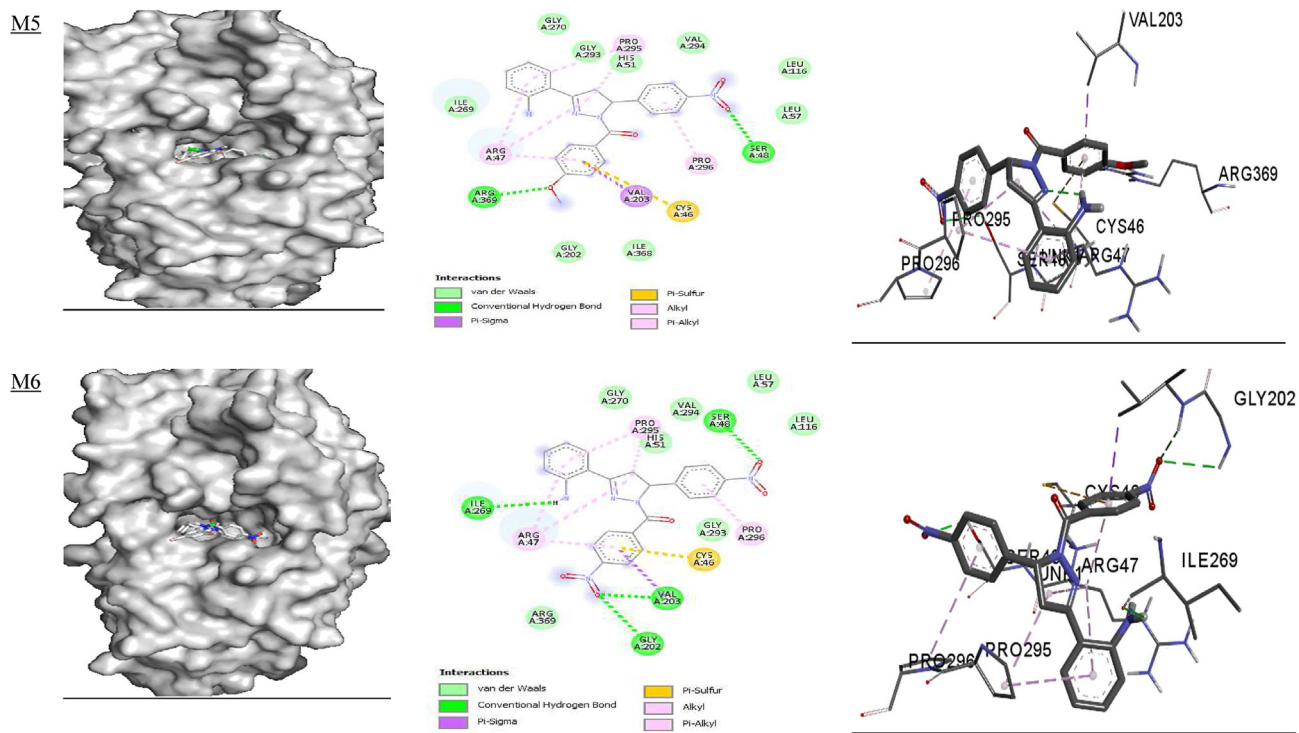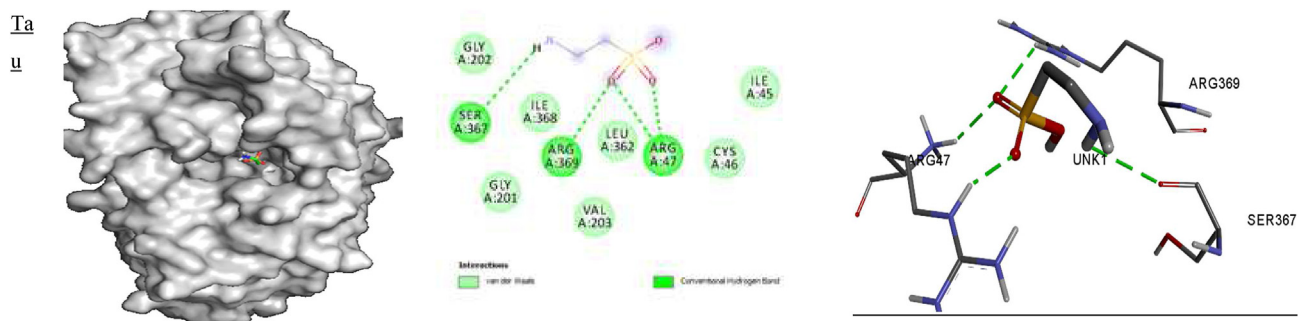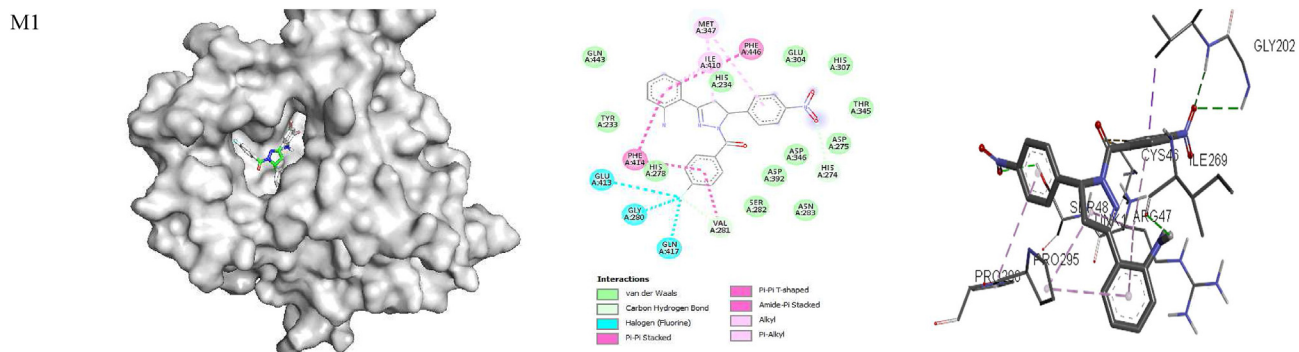


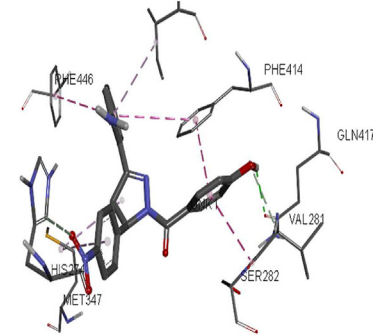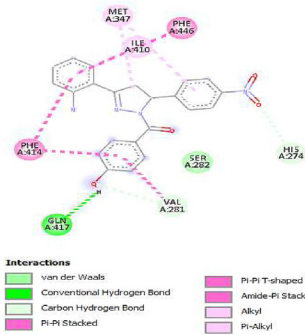**Figure 4:** Docked complexes of the **1RO6** receptor with compounds **M1–M6**, showing interactions in the binding pocket.
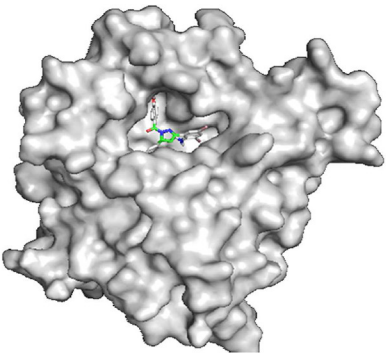
M2



M3
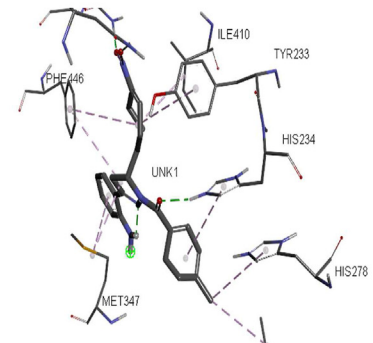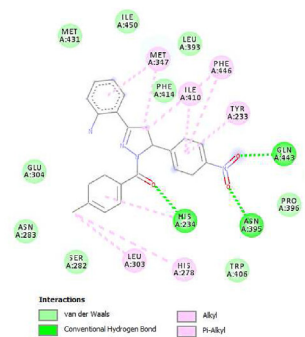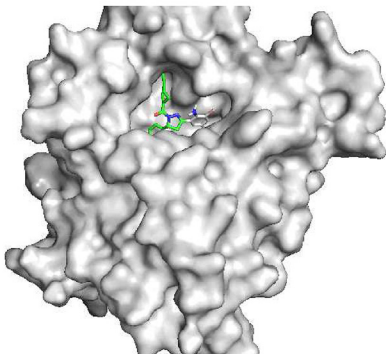


**Figure 4:** continued.

M4



M5



**Figure 4:** continued.

M6

Rolipram
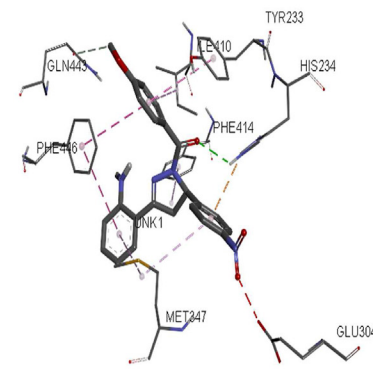


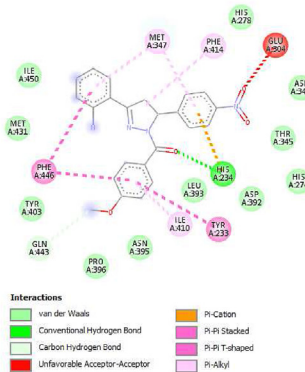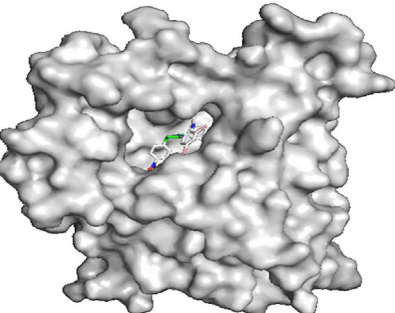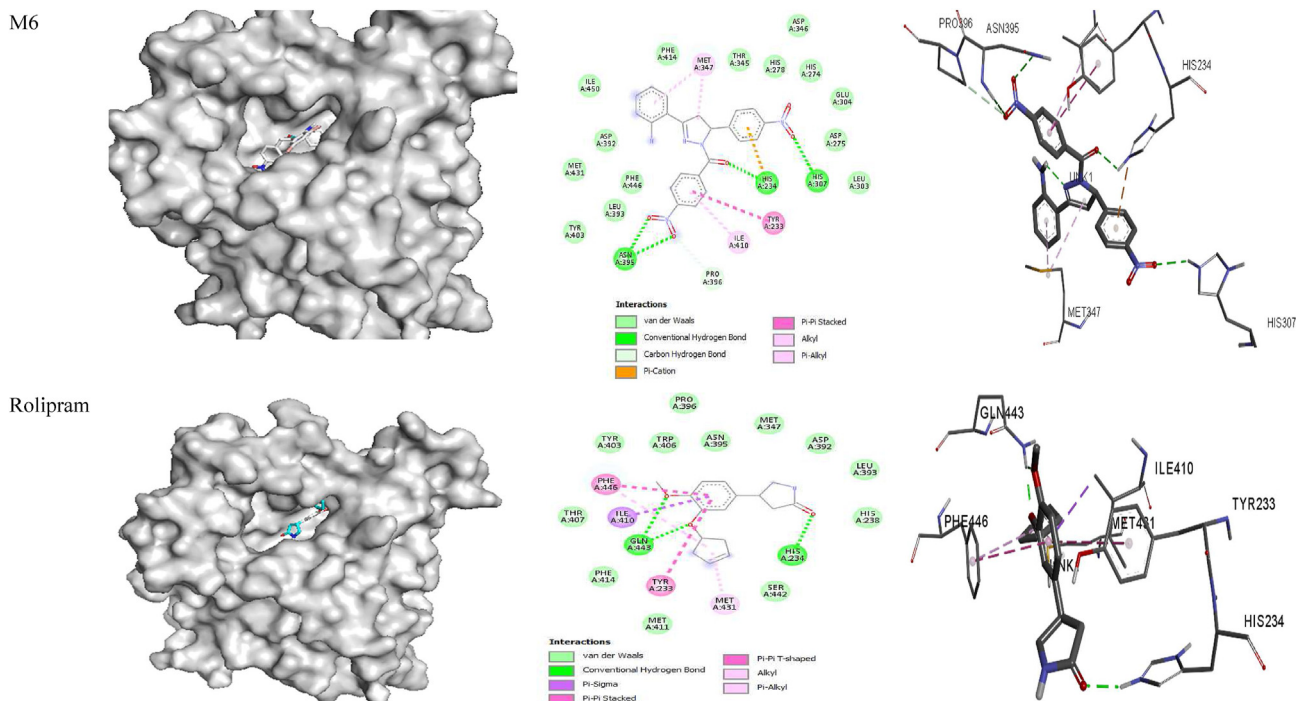**Figure 4:** continued.

414, VAL 281 and PHE 446 are involved in amide-π and π-π T-stacking interactions; GLN 417 forms hydrogen bond interactions; MET 347 forms alkyl-π interactions; and VAL 281 is involved in carbon hydrogen bond interactions with **M4**. MET 347, PHE 414 and ILE 410 form alkyl- π interactions; PHE 446 and TYR 233 are involved in π-π T-stacking and π-π T-stacking interactions; and HIS 234 forms hydrogen bond and π-cationic interactions with **M5**. Moreover, MET 347 and ILE 410 form alkyl-π interactions; ASN 395, HIS 234 and HIS 307 are involved in hydrogen bond interactions; TYR 233 forms π-π stacking interactions; and HIS 234 is involved in π-cationic interactions with **M6.** Rolipram is involved in π-π and π-π T-stacking interactions with PHE 446 and TYR 233; hydrogen bonding with GLN 443 and HIS 234; π-sigma interactions with ILE 410; and alkyl-π interactions with PHE 446 and MET 431 (Table 8 and Figure 4). The free energy for binding of rolipram with PDE (**PDB ID: 1RO6**) in the active pocket was −9.7, −9.2, −9.4, −9.9, −8.5 and −8.9 kcal/mol for **M1−M6,** respectively, whereas −8.8 kcal/mol was calculated for rolipram. These findings suggest that all model compounds except **M5** exhibit PDE inhibitory activity than rolipram drug.

## Conclusion

DFT and molecular docking methods were performed on a set of (4-fluorophenyl)[5-(4-nitrophenyl)-3-phenyl-4,5-dihydro-1*H*-pyrazol-1-yl]methanone derivatives to calculate their molecular properties such as global electrophilicity, electron donating and accepting power, electrostatic charge distribution, and anti-hypertensive and antioxidant activity. The calculated $\omega^+$ revealed that the electrophilic nature of

the compounds was increased by the presence of electron withdrawing groups, and the effect was particularly pronounced in the compound with two $NO_2$ groups, **M6**. MEP analysis showed that amide and nitro groups on the compounds were centers of electrophilic attacks, and the magnitude of the molecular hyperpolarizability suggested that the compounds might have NLO properties.

The binding affinity for the protein-ligand complexes ranged from −8.8 to −9.3 kcal/mol—values higher than that of taurine, an antioxidant involved in inhibition of dehydrogenase (**PDB ID: 5ADH**) in hepatic tissue. For PDE (**PDB: 1RO6**), the binding affinity ranged from −8.5 to −9.9 kcal/mol, whereas that of rolipram, a selective inhibitor of PDE4, was −8.8 kcal/mol, thereby indicating that only **M5** (−8.5 kcal/mol) had a lower binding affinity than rolipram. Thus, the docking results showed that these compounds may be excellent antioxidant and anti-inflammatory agents.

## Source of funding

## Conflict of interest

The authors have no conflict of interest to declare.

## Ethical approval

Not applicable.

## Authors' contributions

SB, OOA, OAK: Conceptualization; OAK, IAO, OTE, AMD: Methodology; IAO, SB, OTE, LDF, OAK, OAD, AIO, AMD and OOA: Writing- Original draft preparation; OAK and AMD: Software and Visualization; OAD and AIO: Data curation; IAO, SB, OTE, LDF, OAK, OAD, AIO, AMD and OOA: Reviewing and Editing; SB, OOA: Supervision: SB: Validation: OAK. All authors have critically reviewed and approved the final draft and are responsible for the content and similarity index of the manuscript.

## References

1. Holzer W, Gruber H. N1-Substituted 3,5-dimethoxy-4-halogeno-1H-pyrazoles: synthesis and NMR study. **J Heterocycl Chem 1995**; 32(4): 1351−1354.

2. Haddad N, Baron J. Novel application of the palladium-catalyzed N-arylation of hydrazones to a versatile new synthesis of pyrazoles. **J Baron Tetrahedron Lett 2002**; 43: 2171−2173. https://doi.org/10.1016/S0040-4039(02)00245-9.

3. Zheng Y, Zheng M, Ling X, Liu Y, Xue Y, An L, Gu N, Jin M. Design, synthesis, quantum chemical studies and biological activity evaluation of pyrazole−benzimidazole derivatives as potent Aurora A/B kinase inhibitors. **Bioorg Med Chem Lett 2013**; 23: 3523−3530. https://doi.org/10.1016/j.bmcl.2013.04.039.

4. Fustero S, Sánchez-Roselló M, Barrio P, Simón-Fuentes A. From 2000 to Mid-2010: a fruitful decade for the synthesis of pyrazoles. **Chem Rev 2011**; 111: 6984−7034.

5. Ansari A, Ali A, Asif M. Biologically active pyrazole derivatives. **New J Chem 2017**; 41: 16−41. https://doi.org/10.1039/C6NJ03181A.

6. Channar PA, Afzal S, Ejaz SA, Saeed A, Larik FA, Mahesar PA, Lecka J, Sévigny J, Erben6 MF, Iqbal J. Exploration of carboxy pyrazole derivatives: synthesis, alkaline phosphatase, nucleotide pyrophosphatase/phosphodiesterase and nucleoside triphosphate diphosphohydrolase inhibition studies with potential anticancer profile. **Euro J Med Chem 2018**. https://doi.org/10.1016/j.ejmech.2018.07.002.

7. Hes RV, Wellinga K, Grosscurt AC. 1-Phenylcarbamoyl-2-pyrazolines: a new class of insecticides. 2. Synthesis and insecticidal properties of 3,5-diphenyl-1-phenylcarbamoyl-2-pyrazolines. **J Agric Food Chem 1978**; 26: 915−918.

8. Azimi F, Ghasemi JB, Azizian H, Najafi M, Faramarzi MA, Saghaei L, Sadeghi-aliabadi H, Larijani B, Hassanzadeh F, Mahdavi M. Design and synthesis of novel pyrazole-phenyl semicarbazone derivatives as potential α-glucosidase inhibitor: kinetics and molecular dynamics simulation study. **Int J Biol Macromol 2018**. https://doi.org/10.1016/j.ijbiomac.2020.10.263.

9. Rahman MA, Siddiqui AA. Pyrazoline derivatives: a worthy insight into the recent advances and potential pharmacological activities. **Int J Pharmaceut Sci Drug Res 2010**; 2: 165−175.

10. Hampp C, Hartzema AG, Kauf TL. Cost-utility analysis of rimonabant in the treatment of obesity. **Value Health 2008**; 11: 389−399. https://doi.org/10.1111/j.1524-733.2007.00281.x.

11. Chaudhry F, Shahid W, al-Rashida M, Ashraf M, Munawar MA, Khan MA. Synthesis of imidazole-pyrazole conjugates bearing aryl spacer and exploring their enzyme inhibition potentials. **Bioorg Chem 2021**; 108:104686.

12. Ahmad G, Rasool N, Qamar MU, Alam MM, Kosar N, Mahmood T, Imran M. Facile synthesis of 4-aryl-N-(5-methyl-1H-pyrazol-3-yl)benzamides via Suzuki Miyaura reaction: antibacterial activity against clinically isolated NDM-1-positive bacteria and their Docking Studies. **Arab J Chem 2021**; 14: 103270.

13. Szukalski A, Sznitko L, Cyprych K, Miniewicz A, Mysliwiec J. Light amplification in derivatives of pyrazoline-based system. **J Phys Chem C 2014**; 118: 8102−181010.

14. Mysliwiec J, Sznitko L, Szukalski A, Parafniuk K, Bartkiewicz S, Miniewicz A, Sahraoui B, Kajzar I Rau F. Amplified spontaneous emission of 3-(1,1-dicyanoethenyl)-1-phenyl-4,5-dihydro-1H-pyrazole molecule embedded in various polymer matrices. **Opt Mater 2012**; 34: 1725−1728.

15. Sznitko L, Mysliwiec J, Parafiniuk K, Palewska K, Bartkiewicz S, Miniewicz A. Amplified spontaneous emission in polymethyl methacrylate doped with 3-(1,1- dicyanoethenyl)-1-phenyl-4,5-dihydro-1H-pyrazole (DCNP). **Chem Phys Lett 2011**; 512: 247−250.

16. Moylan CR, Miller RD, Twieg RJ, Betterton KM, Lee VY, Matray TJ, Nguyen C. Synthesis and nonlinear-optical properties of Donor−Acceptor-substituted triaryl azole derivatives. **Chem Mater 1993**; 5: 1499−1508.

17. Szukalski A, Sznitko L, Cyprych K, Miniewicz A, Mysliwiec J. Light amplification in derivatives of pyrazoline-based systems. **J Phys Chem C 2014**; 118: 8102−8110.

18. Jin M, Liang YJ, Lu R, Chuai XH, Yi ZH, Zhao Y, Zhang HJ. Synthesis and properties of photoluminescence and electroluminescence of pyrazoline derivatives. **Synth Met 2004**; 140: 37−41.

19. Miniewicz A, Palewska K, Karpinski P, Sznitko L, Zielinski M. Fluorescence and SHG in organic nanocrystals of DCNP. **Proc SPIE 2012**; 8464:84640.

20. Fu H-B, Yao J-N. Size effects on the optical properties of organic nanoparticles. **J Am Chem Soc 2001**; 123: 1434−1439.

21. Fuxing G, Lei Z, Xuefeng Y, Limin T. Polymer single-nanowire optical sensors. **Nano Lett 2008**; 8: 2757−2761.

22. Chandrakantha B, Isloor AM, Sridharan K, Philip R, Shetty P, Padaki M. Novel N-substituted-5-phenyl-1H-pyrazole-4-ethyl carboxylates as potential NLO materials. **Arab J Chem 2013**; 6: 97−102.

23. Papagiannouli I, Szukalski A, Iliopoulos K, Mysliwiec J, Courisa S, Sahraoui B. Pyrazoline derivatives with a tailored third order nonlinear optical response. **RSC Adv 2015**; 5: 48363−48367.

24. Zhao P-S, Wang HY, Li RQ, Guo HM. Synthesis, crystal structure, electronic spectra and density functional studies on 1N-phenyl-3-(3,4-dichlorophenyl)-5-phenyl-2-pyrazoline. **J Chin Chem Soc (Taipei, Taiwan) 2008**; 5: 183−188.

25. Udaya Sri N, Chaitanya K, Prasad MVS, Veeraiah V, Veeraiah A. Experimental (FT-IR, FT-Raman and UV-Vis spectra) and density functional theory calculations of diethyl 1Hpyrazole-3,5-dicarboxylate. **J Mol Struct 2012**; 1019: 68−79.

26. Channar PA, Saeed A, Erben MF, Larik FA, Riaz S, Florke U, Arshad M. Synthesis, conformational studies and NBO analysis of (4-chloro-3,5-dimethyl-1H-pyrazol- 1-yl)(p-tolyl)methanone. **J Mol Struct 2019**; 1191: 152−157.

27. Saeed A, Khurshid A, Floerke U, Echeverría GA, Piro OE, Gil DM, Rocha M, Frontera A, Mumtaz A, El-Seedi H, Erben MFF. Intermolecular interactions in antipyrine-like derivatives 2-halo-N-(1,5-dimethyl-3-oxo-2-phenyl-2,3-dihydro-1-H-pyrazol-4-yl)benzamides: X-ray structure, Hirshfeld surface analysis and DFT calculations. **New J Chem 2020**. https://doi.org/10.1039/D0NJ03958F.

28. Bharathi R, Santhi N. Combined experimental and theoretical studies on molecular structures, spectroscopy of 4-(3-(2-amino-3,5-dibromophenyl)-1-(benzoyl)-4,5-dihydro-1H-pyrazol-5-yl)

benzonitriles through NBO, FT-IR, HOMO-LUMO and NLO analyzes. **J Theor Comput Chem 2017**; 16(7):1750057. https://doi.org/10.1142/S0219633617500572.

29. Spartan user's guide, Wave function, Inc, Irvine, CA 92612 USA.

30. Hehre WJ, Radom L, Schleyer PVR, Pope JA. *Ab initio molecular orbital theory*. New York: Wiley; 1988.

31. Becke AD. Density-functional thermochemistry. III. The role of exact exchange. **J Chem Phys 1993**; 98: 5648−5652.

32. Lee C, Yang W, Parr RG. Development of the Colle-Salvetti correlation-energy formula into a functional of the electron density. **Phys Rev B 1988**; 37: 785−789.

33. **Spartan'14** Wavefunction, Inc. Irvine, CA.

34. Andersson MP, Uvdal P. New scale factors for harmonic vibrational frequencies using the B3LYP density functional method with the triple-œ basis set 6−311+G(d,p). **J Phys Chem A 2005**; 109: 2937−2941.

35. Delgado-Montiel T, Baldenebro-Lopez J, Soto-Rojo R, Glossman-Mitnik D. Quantum chemical study of the effect of π-bridge on the optical and electronic properties of sensitizers for DSSCs incorporating dioxythiophene and thiophene units. **Theor Chem Acc 2016**; 135: 235.

36. Delgado-Montiel T, Baldenebro-Lopez J, Soto-Rojo R, Glossman-Mitnik D. Theoretical study of the effect of π-bridge on optical and electronic properties of carbazole-based sensitizers for DSSCs. **Molecules 2020**; 25: 3670.

37. Parr RG, Szentpaly L, Liu S. Electrophilicity index. **J Am Chem Soc 1999**; 121(9): 1922−1924.

38. Gazquez JL, Cedillo A, Vela A. Electrodonating and electro-accepting powers. **J Phys Chem 2007**; 111: 1966−1970.

39. Zhao D, Lu Q, Su R, Li Y, Zhao M. Light harvesting and optical-electronic properties of two quercitin and rutin natural dyes. **Appl Sci 2019**; 9(2019): 2567.

40. Shimaa AH. TD-DFT calculations, electronic structure, natural bond orbital analysis, nonlinear optical properties electronic absorption spectra and antimicrobial activity application of new bis-spiropipridinon/pyrazole derivatives. **Eur J Chem 2018**; 9(4): 287−302.

41. El-shishtawy RM, Abdullah MA, Saadullah GA, Shaaban AKE. Molecular design of donor-acceptor dyes for efficient dye-sensitized solar cells I: a DFT study. **J Mol Model 2014**; 20(6): 2241−2245. https://doi.org/10.1007/s00894-014-2241-5.

42. Irfan A, Muhammad S, Alsehemi AG, Al-Assiri MS, Chaudhry AR. The effect of anchoring groups on the electro-optical and charge injection in triphenylamine derivatives-$Ti_6O_{12}$. **J Theor Comput Chem 2015**; 14(4):1550027. https://doi.org/10.1142/S0219633615500297.

43. Kim B-G, Zhen C-G, Jeong EJ, Kieffer J, Kim J. Organic dye design tools for efficient photocurrent generation in dye-sensitized solar cells: exciton binding energy and electron acceptors. **Adv Funct Mater 2012**; 22: 1606−1612.

44. Semire B, Oyebamiji AK, Odunola AO. Tailoring of energy levels in (2Z)-2-cyano-2-[2-[(E)-2-[2-[(E)-2-(p-tolyl)vinyl]thieno[3,2-b]thiophen-5-yl]vinyl]pyran-4-ylidene]acetic acid derivatives via conjugate bridge and fluorination of acceptor units for effective D-π-A dye-sensitized solar cells: DFT-TDDFT approach. **Res Chem Intermed 2017**; 43: 1863−1879. https://doi.org/10.1007/s11164-016-2735-0.

45. Omri N, Yahyaoui M, Banani R, Messaoudi S, Moussa F, Abderrabba M. *Ab-initio* HF and density functional theory investigations on the synthesis mechanism, conformational stability, molecular structure and UV spectrum of N0-Formylkynurenine. **J Theor Comput Chem 2016**; 15:1650006.

46. Kosar B, Albayrak C. Spectroscopic investigations and quantum chemical computational study of (E)-4-methoxy-2-[(p-tolylimino)methyl]phenol. **Spectrochim Acta 2011**; 78: 160−167.

47. Bouzayen N, Mbarek M, Alimi K. Solvent effects on optical and electronic properties of carbazolebenzothiazole based bipolar compound: TD-DFT/PCM approach. **Comput Theor Chem 2015**; 3(1): 28−39.

48. Kumar MD, Rajesh P, Dharsini RP, Inban ME. Molecular geometry, NLO, MEP, HOMO-LUMO and mulliken charges of substituted piperidine phenyl hydrazines by using density functional theory. **Asian J Chem 2020**; 32(2): 401−407.

49. Semire B, Bello IA. Density functional theory (DFT) study on structural and electronic properties of disperse dyes derived from 2-amino-4-trifluoromethylbenzothiazole and N, N-alkylanilines. **Int J Appl Chem 2013**; 9: 151−163.

50. Semire B, Odunola OA. DFT study on low molecular weight α,α-*Ditert*-butyl-4h-cyclopenta[2,1-b,3;4-b']dithiophene and α,α-*ditert*-butyl-4h-Cyclopenta[2,1-B,3;4-B']Dithiophene S-oxide bridged derivatives. **Quim Nova 2014**; 37(5): 833−8384.

51. Raftani M, Abram T, Bennani MN, Bouachrine M. Theoretical study of new conjugated compounds with a low bandgap for bulk heterojunction solar cells: DFT and TD-DFT study. **Res Chem 2020**; 2:100040. https://doi.org/10.1016/j.rechem.2020.100040.

52. Arockia doss M, Savithiri S, Rajarajan G, Thanikachalam V, Saleem H. Synthesis, spectroscopic (FT-IR, FT-Raman, UV and NMR) and computational studies on 3tpentyl-2r,6c diphenylpiperidin-4-one semicarbazone. **Spectrochim Acta 2015**; 148: 189−202.

53. Chahkandi M, Bhatti MH, Yunus U, Shaheen S, Nadeem M, NawazTahir M. Synthesis and comprehensive structural studies of a novel amide based carboxylic acid derivative: non covalent interactions. **J Mol Struct 2017**; 1133: 499−509.

54. Anbu V, Vijayalakshmi KA. Quantum chemical studies on the spectroscopic, electronic structural and nonlinear properties of an organic N-methyl-N-(2,4,6-Trinitrophenyl) nitramide energetic molecule. **J Curr Phys Chem 2019**; 9: 5−21.

55. Silverstein RM, Webster FX. *Spectroscopic identification of organic compounds*. 7th ed. New York: Wiley; 2005.

56. Srinivasan P, David SA. DFT and Bader's AIM analysis of 2, 5, diphenyl-1, 3, 4-oxadiazole molecule: a organic light emitting diode (OLED). **J Theor Comput Chem 2015**; 14:1550038. https://doi.org/10.1142/S0219633615500388.

57. Jin ZM, Zhao B, Zhou W, Jin Z. X-ray powder diffraction analysis of a nonlinear optical material o−chlorobenzol−benzoyl thiourea. **Power Diffra 1997**; 12: 47−48. https://doi.org/10.1017/S0885715600009428.

58. Semire B, Larayetan AR. Ab initio and DFT study on molecular structure, reactivity indices and nonlinear properties of 4-(4-aminophenylethynyl)picolinic acid and 4-(3-aminophenylethynyl)picolinic acid. **Iraqi Nat J Chem 2016**; 16: 224−242.

59. Karrouchi K, Brandán SA, Sert Y, El Karbane M, Radi S, Ferbinteanu M, Garcia Y, Ansar M. Synthesis, structural, molecular docking and spectroscopic studies of (E)-N'-(4-methoxybenzylidene)-5-methyl-1H-pyrazole-3-carbohydrazide. **J Mol Struct 2021**; 1225:129072.

60. Zaccolo M, Movsesian MA. cAMP and cGMP signaling cross-talk: role of phosphodiesterases and implications for cardiac pathophysiology. **Circ Res 2007**; 100(11): 1569−1578. https://doi.org/10.1161/CIRCRESAHA.106.144501.

61. Bender AT, Beavo JA. Cyclic nucleotide phosphodiesterases: molecular regulation to clinical use. **Pharmacol Rev 2006**; 58: 488−520.

62. Xu RX, Rocque WJ, Lambert MH, Vanderwall DE, Luther MA, Nolte RT. Crystal structures of the catalytic domain of phosphodiesterase 4B complexed with AMP, 8-Br-AMP, and rolipram. **J Mol Biol 2004**; 337: 355−365.

63. Kim HK, Kwon JY, Yoo C, Abdi S. The analgesic effect of rolipram, a phosphodiesterase 4 inhibitor, on chemotherapy-

induced neuropathic pain in rats. **Anesth Analg 2015**; 121: 822–828.

64. Raker VK, Becker C, Steinbrink K. The cAMP pathway as therapeutic target in autoimmune and inflammatory diseases. **Front Immunol 2016**; 7(2016): 123. https://doi.org/10.3389/fimmu.2016.00123.

65. Lobo V, Patil A, Phatak A, Chandra N. Free radicals, antioxidants and functional foods. **Impact Human Health 2010**; 4(8): 118–126. https://doi.org/10.4103/0973-7847.70902.

66. Young IS, Woodside JV. Antioxidants in health and disease. **J Clin Pathol 2001**; 54(2001): 176–186.

67. Ser H-L, Palanisamy UD, Yin W-F, AbdMalek SN, Chan K-G, Goh B-H, Lee L-H. Presence of antioxidative agent, Pyrrolo [1,2-a]pyrazine-1,4-dione, hexahydro- in newly isolated *Streptomyces mangrovisoli* sp. nov. **Front Microbiol 2015**; 6: 854. https://doi.org/10.3389/fmicb.2015.00854.

68. Stepanić V, Matijašić M, Horvat T, Verbanac D, Kučerová-Chlupáčová M, Saso L, Žarković N. Antioxidant activities of alkyl substituted pyrazine derivatives of chalcones—in vitro and in silico study. **Antioxidants 2019**; 8: 90. https://doi.org/10.3390/antiox8040090.

69. Kitawata BS, Singh M. Synthesis, characterization, antibacterial, antioxidant, DNA binding and SAR study of novel pyrazine moiety bearing 2-pyrazoline derivatives. **New J Chem 2014**; 38: 4290–4299.

70. Bouckenooghe T, Remacle C, Reusens B. Is taurine a functional nutrient? **Curr Opin Clin Nutr Metab Care 2006**; 9: 728–733. https://doi.org/10.1097/01.mco.0000247469.26414.55.

71. Sirdah MM. Protective and therapeutic effectiveness of taurine in diabetes mellitus: a rationale for antioxidant supplementation. **Diabetes Metabol Syndr 2015**; 9: 55–64. https://doi.org/10.1016/j.dsx.2014.05.001.

72. Murakami S. Role of taurine in the pathogenesis of obesity. **Mol Nutr Food Res 2015**; 59: 1353–1363. https://doi.org/10.1002/mnfr.201500067.

73. Franconi F, Bennardini F, Mattana A, Miceli M, Ciuti M, Mian M, Gironi A, Anichini R, Seghieri G. Plasma and platelet taurine are reduced in subjects with insulin-dependent diabetes mellitus: effects of taurine supplementation. **Am J Clin Nutr 1995**; 61(5): 1115–1119. https://doi.org/10.1093/ajcn/61.4.1115.

74. Sak D, Erdenen F, Müderrisoglu C, Altunoglu E, Sozer V, Gungel H, Guler PA, Sak T, Uzun H. The relationship between plasma taurine levels and diabetic complications in patients with type 2 diabetes mellitus. **Biomolecules 2019**; 9: 96. https://doi.org/10.3390/biom9030096.

75. Maleki V, Mahdavi R, Hajizadeh-Sharafabad F, Alizadeh M. The effects of taurine supplementation on oxidative stress indices and inflammation biomarkers in patients with type 2 diabetes: a randomized, double-blind, placebo-controlled trial. **Diabetol Metab Syndrome 2020**; 12: 9. https://doi.org/10.1186/s13098-020-0518-7.

76. Trott O, Olson AJ. AutoDockVina: improving the speed and accuracy of docking with a new scoring function, efficient optimization and multithreading. **J Comput Chem 2010**; 31: 455–561. https://doi.org/10.1002/jcc.21334.

77. Oyebamiji AK, Fadare OA, Akintelu SA, Semire B. Biological studies on Anthra[1,9-cd]pyrazol-6(2D)-one analogues as anti-vascular endothelial growth factor via in silico mechanisms. **Chem Afr 2021**; 4: 955–963. https://doi.org/10.1007/s42250-021-00276-2.

78. Adegbola PI, Semire B, Fadahunsi OS, Adegoke AE. Molecular docking and ADMET studies of *Allium cepa, Azadirachta indica* and *Xylopia aethiopica* isolates as potential anti-viral drugs for Covid-19. **Virus Dis 2021**; 32: 85–97. https://doi.org/10.1007/s13337-021-00682-7.

79. Adegbola AE, Fadahunsi OS, Alausa A, Abijo AZ, Balogun TA, Aderibigbe TS, Semire B, Adegbola PI. Computational prediction of nimbanal as potential antagonist of respiratory syndrome coronavirus. **Inform Med Unlocked 2021**; 24: 100617. https://doi.org/10.1016/j.imu.2021.100617.

80. Yonas B, Alfred M, Paballo L, Oyebamiji AK, Adedapo SA, Thierry YF, Lesetja RM. Molecular hybrid of 1,2,3-triazole and schiff base as potential antibacterial agents: DFT, molecular docking and ADME studies. **J. Mol. Struct. 2023**; 1286: 135617.

81. Kramer B, Rarey M, Lengauer T. Evaluation of the FlexX incremental construction algorithm for protein ligand docking. **Proteins Struct Funct Genet 1999**; 37: 228–241.

82. El-Azab AS, Mary YS, Panicker CY, Abdel-Aziz AAM, El-Sherbeny MA, Van Alsenoy C. DFT and experimental (FT-IR and FT-Raman) investigation of vibrational spectroscopy and molecular docking studies of 2-(4-oxo-3-phenethyl-3,4-dihyroquinazolin-2-ylthio)-N-(3,4,5-trimethoxyphenyl) acetamide. **J Mol Struct 2016**; 1113: 133–145. https://doi.org/10.1016/j.molstruc.2016.02.038.

83. Adegbola PI, Fadahunsi OS, Adegbola AE, Semire B. *In silico* studies of potency and safety assessment of selected trial drugs for the treatment of COVID-19. **Silico Pharmacol 2021**; 9: 45. https://doi.org/10.1007/s40203-021-00105-x.

84. Adepoju AJ, Latona DF, Olafare OG, Oyebamiji AK, Abdul-Hammed M, Semire B. Molecular docking and pharmacokinetics studies of (Curcumin) potency against Ebola virus. **Ovidius Univ Ann Chem 2022**; 33: 22–35.

85. Mahmudov I, Demir Y, Sert Y, Abdullayev Y, Sujayev A, Alwasel SH, Gulcin I. Synthesis and inhibition profiles of N-benzyl- and N-allyl aniline derivatives against carbonic anhydrase and acetylcholinesterase — a molecular docking study. **Arab J Chem 2022**; 15:103645.

86. Channar PA, Afzal S, Ejaz SA, Saeed A, Larik FA, Mahesar PA, Lecka J, Sévigny J, Erben MF, Iqbal J. Exploration of carboxy pyrazole derivatives: synthesis, alkaline phosphatase, nucleotide pyrophosphatase/phosphodiesterase and nucleoside triphosphate diphosphohydrolase inhibition studies with potential anticancer profile. **Euro J Med Chem 2018**. https://doi.org/10.1016/j.ejmech.2018.07.002.

87. Ibrahim AO, Semire B, Adepoju AJ, Latona DF, Oyebamiji AK, Owonikoko AD, Oladuji TE, Odunola OA. In Silico investigations on structure, reactivity indices, NLO properties, and bio-evaluation of 1-benzyl-2-phenyl-1H-benzimidazole derivatives using DFT and molecular docking approaches. **Biointer Res Appl Chem 2023**; 13: 233. https://doi.org/10.33263/BRIAC133.233.